1 **Title:** Tuning of Delta-Protocadherin Adhesion Through Combinatorial Diversity

2

3 **Author names and affiliations:** Adam J. Bisogni[1], Shila Ghazanfar[2], Eric O.

4 Williams[1,3], Heather M. Marsh[1], Jean Y. H. Yang[2], David M. Lin[1*]

5

6 [1]Department of Biomedical Sciences, Cornell University, Ithaca, NY 14853

7 [2]School of Mathematics and Statistics, The University of Sydney, Australia

8 [3]Department of Biology & Chemistry, Fitchburg State University, Fitchburg, MA 01420

9

10 *Correspondence: dml45@cornell.edu

11   **Abstract**

13   The delta-protocadherins (δ-Pcdhs) play key roles in neural development, and
14   expression studies suggest they are expressed in combination within neurons. The
15   extent of this combinatorial diversity, and how these combinations influence cell
16   adhesion, is poorly understood. We show that individual mouse olfactory sensory
17   neurons express 0-7 δ-Pcdhs. Despite this apparent combinatorial complexity, K562 cell
18   aggregation assays revealed simple principles mediate tuning of δ-Pcdh adhesion. Cells
19   can vary the number of δ-Pcdhs expressed, the level of surface expression, and which
20   δ-Pcdhs are expressed, as different members possess distinct apparent adhesive
21   affinities. These principles contrast with those identified previously for the clustered
22   protocadherins (cPcdhs), where the particular combination of cPcdhs expressed does
23   not appear to be a critical factor. Despite these differences, we show δ-Pcdhs can
24   modify cPcdh adhesion. Our studies show how intra- and interfamily interactions can
25   greatly amplify the impact of this small subfamily on neuronal function.

Introduction

The delta-protocadherins (δ-Pcdhs) are a nine-member subfamily of the cadherin superfamily (Hulpiau and van Roy, 2009; Nollet et al., 2000), and play diverse roles during neural development. Mutagenesis studies have shown individual δ-Pcdhs are important for neural development, including hindbrain formation, axon guidance, and synaptogenesis (Cooper et al., 2015; Emond et al., 2009; Hayashi et al., 2014; Hoshina et al., 2013; Leung et al., 2013; Light and Jontes, 2017; Uemura et al., 2007; Williams et al., 2011). In humans, mutations in *PCDH19* are the causative basis of one form of epilepsy (Dibbens et al., 2008), and other δ-Pcdhs are implicated in various neurological disorders (Chang et al., 2018; Consortium on Complex Epilepsies, 2014; Morrow et al., 2008).

How does this relatively small gene family mediate these varied effects? While significant effort has been devoted towards characterizing the role of individual δ-Pcdhs in neural development, almost nothing is known regarding how multiple family members function together. The δ-Pcdh subfamily has been further divided into the δ-1 (*Pcdh1*, *Pcdh7*, *Pcdh9*, and *Pcdh11*) and δ-2 (*Pcdh8*, *Pcdh10*, *Pcdh17*, *Pcdh18*, and *Pcdh19*) subfamilies based on differences in the number of extracellular domains and also the intracellular domain (Redies et al., 2005; Vanhalst et al., 2005). Double label RNA *in situ* hybridization studies indicate individual neurons express more than one δ-Pcdh (Etzrodt et al., 2009; Krishna-K et al., 2011). This suggests a model where different combinations of δ-Pcdhs may be expressed within different populations of neurons. Whether such combinations exist or how many δ-Pcdhs may be expressed per neuron is still not known. It seems reasonable, however, to postulate that combinatorial expression would greatly enhance the impact of δ-Pcdhs on cellular function. If such combinations exist, it is also unknown how they would influence or modify δ-Pcdh-mediated adhesion.

The importance of examining intrafamily δ-Pcdh interactions was recently underscored by a study examining the role of δ-Pcdh adhesion in *PCDH19*-GCE (girls clustering epilepsy), a form of epilepsy limited to females. Pederick et al. demonstrated that mutations in *PCDH19*, a δ-2 family member, affected cell sorting in both *in vitro* aggregation assays and in brains of mice. Furthermore, they also showed that humans with *PCDH19*-GCE exhibit abnormal cortical folding patterns (Pederick et al., 2018). Importantly, they noted that PCDH19 is likely to be co-expressed with other δ-Pcdh family members, and tested how expressing PCDH10 and/or PCDH17 with PCDH19 affected sorting behavior in aggregation assays. In each case, the observed cell sorting behavior varied depending upon which δ-Pcdhs were co-expressed.

But while this study hinted at the combinatorial nature of δ-Pcdh interactions, it did not define the extent of such combinations *in vivo.* More importantly, it did not establish any guiding principles for δ-Pcdh adhesion, or how different combinations influence adhesion. Nevertheless, it underscored the need to define intrafamily interactions in order to understand how loss of *Pcdh19* can influence function.

71 Here, we uncover principles used by the δ-Pcdhs to regulate combinatorial adhesion.
72 We first used single color and double label RNA *in situ* hybridization to show that
73 olfactory sensory neurons (OSNs) are likely to express different combinations of δ-
74 Pcdhs. We next employed single cell RNA analysis to establish the scope of these
75 combinations, and find individual OSNs express between zero and seven δ-Pcdhs. We
76 then systematically address the impact of this combinatorial diversity on intrafamily
77 interactions by utilizing cell aggregation assays. In striking contrast to what has been
78 seen for the clustered protocadherins (cPcdhs; (Thu et al., 2014)), we observed a range
79 of potential adhesive behaviors. We were able to define fundamental principles that
80 regulate these outcomes. In combination, these principles provide cells with a powerful
81 means of fine tuning their adhesive interactions with other cells. Finally, we show that δ-
82 Pcdhs can also modify the adhesive function of cPcdhs, which have been shown to be
83 important for neuronal survival, dendritogenesis, synapse formation, and self-avoidance
84 (Lefebvre et al., 2012; Molumby et al., 2016; Wang et al., 2002; Weiner et al., 2005).
85 These results provide an initial glimpse into interfamily interactions among
86 protocadherin subfamilies. Our studies therefore provide a framework for determining
87 how combinations of δ-Pcdhs mediate adhesion, and also lay the foundation for
88 understanding how different cadherin subfamilies integrate to regulate cell-cell
89 adhesion.
90
91 **Results**
92
93 **Defining Combinatorial Expression of δ-Pcdhs In Single Neurons**
94 We first performed single color RNA *in situ* hybridization to examine δ-Pcdh expression
95 in the olfactory epithelium (Figure 1 - Supplement 1A-G). All detectable δ-Pcdhs were
96 expressed in a punctate pattern, indicating differential expression among OSNs.
97 Interestingly, the expression pattern for any given δ-Pcdh was not uniform throughout
98 the epithelium. For example, *Pcdh1* is more highly expressed in the lateral epithelium,
99 and more weakly medially (Figure 1 - Supplement 1B,C). In both regions the expression
100 was clearly punctate, but greater numbers of OSNs in the lateral epithelium expressed
101 *Pcdh1*. In contrast, other δ-Pcdhs, such as *Pcdh9* and *Pcdh17*, show the opposite
102 pattern, and are more strongly expressed medially with relatively low expression
103 laterally (Figure 1 - Supplement 1D-G). Differences between δ-1 and δ-2 family
104 members could not be distinguished based upon these patterns. These patterns are
105 essentially maintained as development proceeds, although subtle changes in
106 expression did occur. One exception was *Pcdh10*, whose expression we previously
107 demonstrated to be dependent upon odorant-mediated activity (Williams et al., 2011).
108
109 The δ-Pcdhs are therefore expressed in regional patterns that overlap one another,
110 suggesting combinatorial expression. We used double label RNA *in situ* hybridization to
111 begin testing this hypothesis (Figure 1A). We systematically assayed all expressed
112 pairs to show that 5-35% of olfactory sensory neurons (OSNs) co-express any two δ-
113 Pcdhs (Figure 1 - Supplement 1H). Interestingly, the degree of co-expression varied
114 within the family. For example, *Pcdh1* and *Pcdh7* were only co-expressed 8% of the
115 time, while *Pcdh8* and *Pcdh9* were co-expressed 35% of the time.
116

117 As has been well-established, OSNs expressing the same odorant receptor project to
118 common targets within the olfactory bulb (Ressler et al., 1994; Vassar et al., 1994).
119 Mutant analysis of members of the δ-Pcdh and cPcdh subfamilies has previously shown
120 these genes are important for OSN targeting (Hasegawa et al., 2008; Mountoufaris et
121 al., 2017; Williams et al., 2011). Interestingly, however, not all OSN populations were
122 equally affected. Why some populations expressing a particular odorant receptor were
123 more strongly affected in the mutant than those expressing a different receptor is
124 unknown. We theorized that different OSN populations may express different
125 combinations of δ-Pcdhs. Changes in these combinations would therefore affect cell
126 adhesion mediated by the δ-Pcdhs. We therefore performed a second double label RNA
127 *in situ* hybridization series to survey which δ-Pcdhs are co-expressed among OSNs
128 expressing a given odorant receptor. For any one δ-Pcdh, we examined on average ~70
129 cells expressing a given odorant receptor to determine the degree of overlap (Figure
130 1B,C).
131
132 Confocal analysis showed all five OSN populations surveyed express varying
133 proportions of different δ-Pcdhs (Figure 1B,C). There were striking differences in
134 expression of δ-Pcdhs among the different OSN populations, arguing for the presence
135 of specific combinations of δ-Pcdhs within each population. Interestingly, we did not find
136 a simple one-to-one correspondence between odorant receptor expression and δ-Pcdh
137 expression. Instead, different OSN populations varied in the proportion of δ-Pcdhs they
138 expressed. For example, *Pcdh9* was expressed by more than half of all OSNs
139 expressing *Olfr558*. In contrast, ~12% of *Olfr557* OSNs expressed *Pcdh9*. The variation
140 in δ-Pcdh expression within OSN populations indicates additional levels of regulation
141 must exist. Nevertheless, different OSN populations clearly possess differences in the
142 proportion of δ-Pcdhs expressed by those OSNs. Such differences could be important
143 for defining how δ-Pcdhs mediate targeting.
144
145 We next used the NanoString nCounter platform (Geiss et al., 2008) to more precisely
146 define the extent of co-expression. We isolated 50 randomly selected OSNs, and
147 performed single neuron RNA analysis for δ-Pcdhs and a subset of other genes. A heat
148 map of the raw NanoString data showed strong heterogeneity among OSNs (Figure
149 1D). To classify δ-Pcdhs as being "on" or "off" in a neuron, we used a constrained
150 gamma-normal mixture model (Ghazanfar et al., 2016) (Figure 1 - Supplement 1I). This
151 revealed that individual OSNs expressed anywhere from zero to seven δ-Pcdhs (Figure
152 1E), far exceeding prior estimates based on RNA *in situ* studies. We were unable to
153 determine if there was any preference for co-expression among or between the δ-1 or δ-
154 2 subfamilies.
155
156 We performed several validation experiments (see Validation of NanoString data, Figure
157 1F, and Figure 1 – Supplement 1J), including qRT-PCR on individual OSNs. The
158 observed "on" or "off" expression pattern of this particular validation experiment was
159 highly similar to our NanoString results (Figure 1F). We chose NanoString because we
160 hypothesized a targeted approach would be more sensitive than single cell RNA-seq,
161 which is often limited by low capture efficiency of mRNA (Islam et al., 2011; Marinov et

162 al., 2014). Subsequent comparison with single OSN RNA-seq data sets confirmed this
163 hypothesis (Figure 1 - Supplement 1K,L).
164
165 **Figure 1**
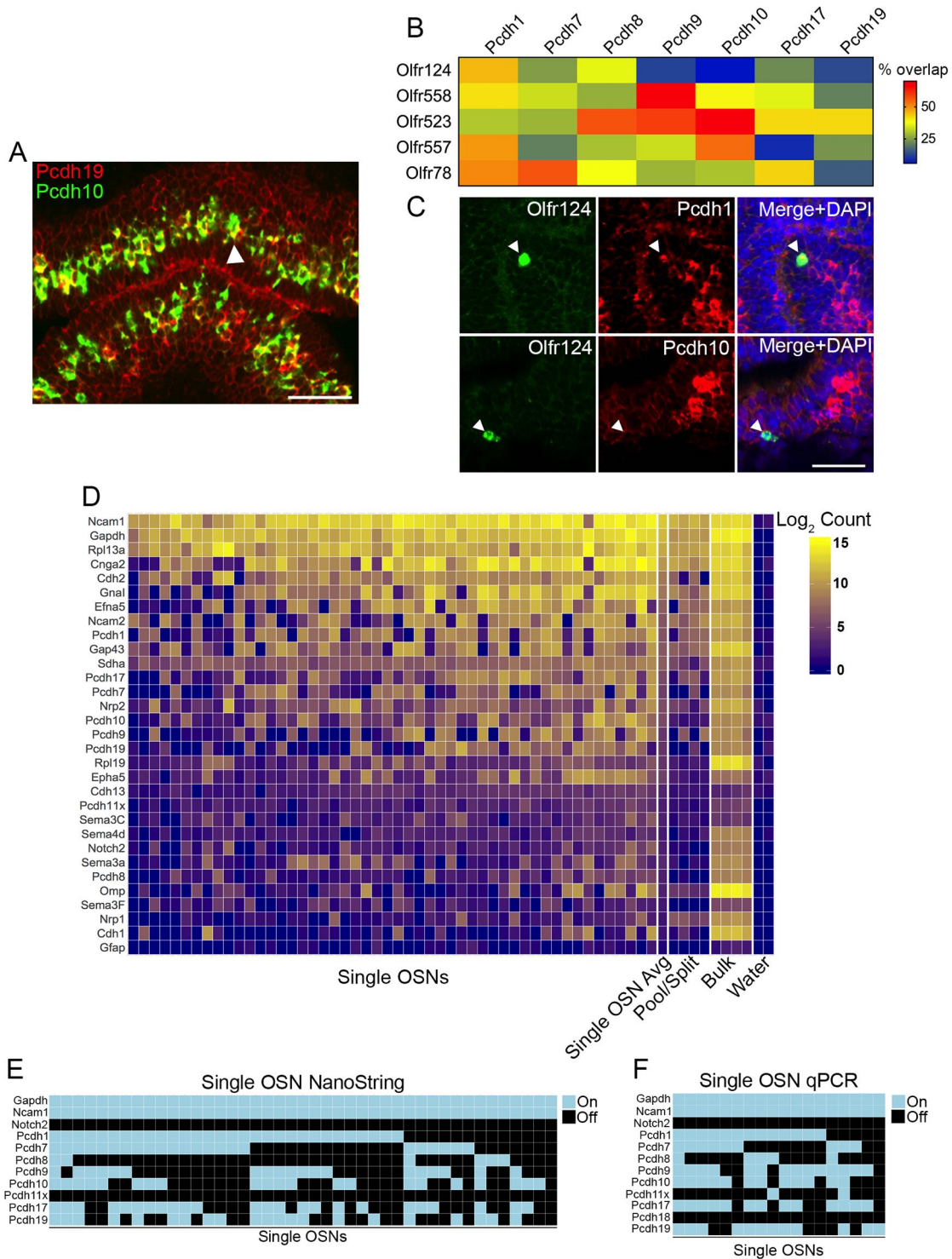
Figure 1. Combinatorial Expression of δ-Protocadherins in Mouse Olfactory Sensory Neurons (OSNs)

(A) Representative image of a double label RNA *in situ* hybridization with *Pcdh19* (red) and *Pcdh10* (green) in E17.5 olfactory epithelium. Both probes are co-expressed in a subset of neurons (arrowheads). Scale bar, 50 μm.

(B) Heat map showing the percentage of co-expression among δ-Pcdhs and OSNs expressing one of five different odorant receptors. The color intensity indicates the percent of co-expression for any one δ-Pcdh with a given receptor.

(C) Representative confocal images of *Olfr124* positive OSNs co-expressed with *Pcdh1* (top row) but not *Pcdh10* (bottom row). Arrowhead indicates location of *Olfr124* positive OSN. Scale bar, 50 μm.

(D) Heat map of $\log_2$ transformed NanoString counts.

(E) Constrained gamma-normal mixture modeling analysis shows individual, randomly selected OSNs express zero to seven δ-Pcdhs.

(F) qRT-PCR of randomly selected single OSNs shows a mosaic pattern of δ-Pcdh expression similar to the NanoString data.
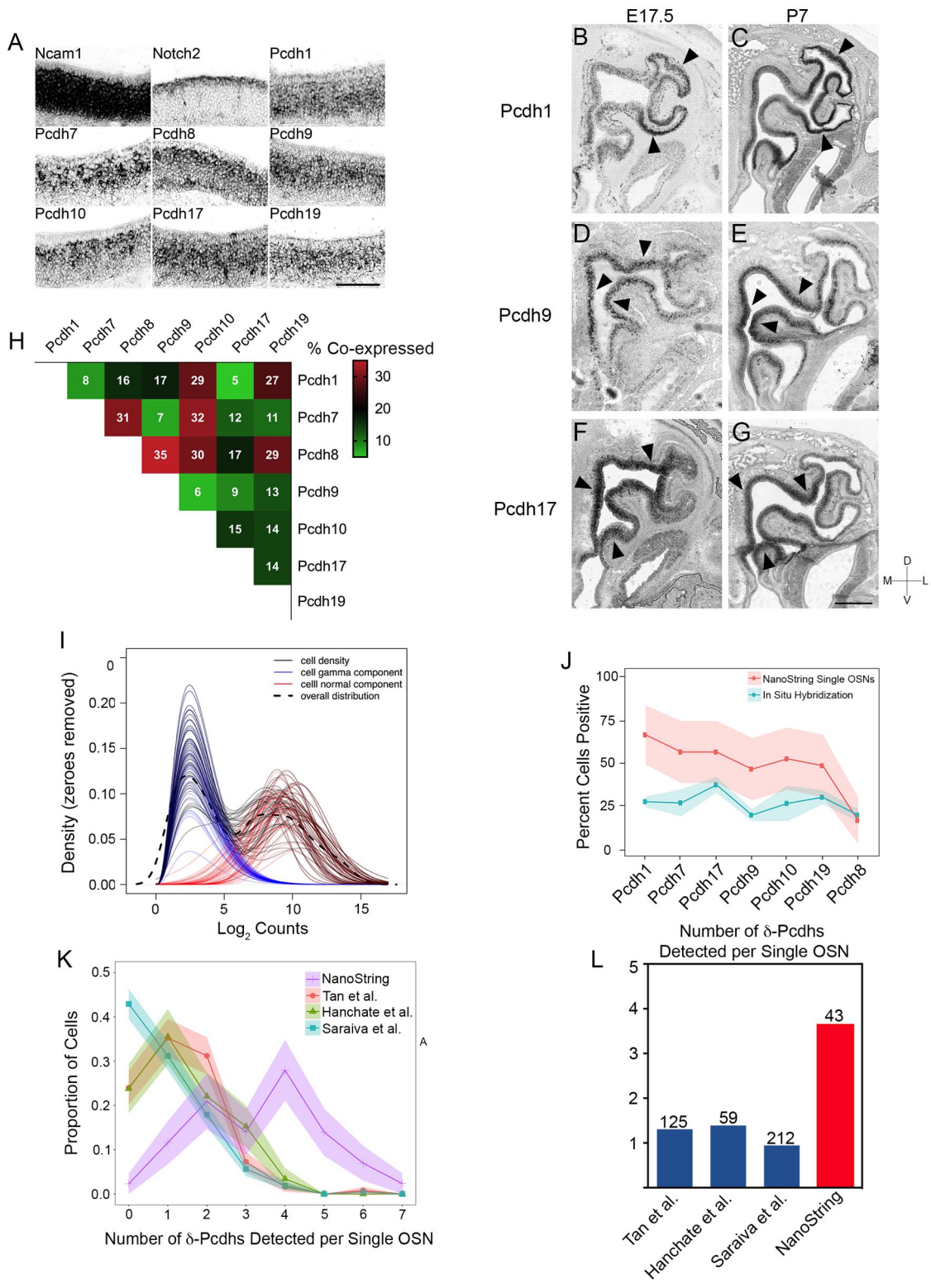
Figure 1 – Supplement 1

Figure 1 - Supplement 1. Expression of δ-Pcdhs in OSNs
(A) Single color RNA *in situ* hybridization of *Ncam1* (a marker of OSNs), *Notch2* (a marker of non-neuronal sustentacular cells), and δ-Pcdhs in P7 olfactory epithelium. Note punctate expression of δ-Pcdhs. Scale bar, 100 µm. *Pcdh11x* and *Pcdh18* could not be detected.
(B-G) Single color RNA *in situ* hybridization of *Pcdh1*, *Pcdh9*, and *Pcdh17* in E17.5 (B,D,F) and P7 (C,E,G) olfactory epithelia. Arrowheads indicate areas of enriched regional expression. Scale bar, 400 µm for (B,D,F) and 500 µm (for C,E,G).
(H) Confocal analysis of a round robin double label RNA *in situ* hybridization series from E17.5 olfactory epithelia. Values indicate percent overlap in OSNs for any given pair. *Pcdh11x* and *Pcdh18* could not be detected with this approach.
(I) Constrained gamma-normal mixture modeling was used to determine if expression of a given gene was "on" or "off" within a given cell. Each line represents a density plot from the model for a single cell. Blue curves represent the lowly expressed component (e.g. "off"), which was allowed to vary in relative proportion but with constant mean and variance parameters. Red curves represent the highly expressed component (e.g. "on") as a normal distribution with variable mean and variance parameters. The dashed curve represents the sample density of all cells across all genes.
(J) Ribbon plot comparing percentage of OSNs expressing a given δ-Pcdh as determined by NanoString (red line) and quantification of RNA *in situ* hybridization signal (blue line). Similar trends were observed for both methods, suggesting enzymatic dissociation during OSN isolation did not greatly alter δ-Pcdh expression. Shaded regions represent 95% CI.
(K) Ribbon plot comparing δ-Pcdh expression in single OSNs as detected by NanoString and three different single OSN RNA-seq studies. Data from RNA-seq studies were re-analyzed using the constrained gamma-normal mixture modeling approach. Cells were first filtered based on positive gene expression of *Ncam1* to parallel the selection of *Ncam1* positive OSNs used in this study. The three single OSN RNA-seq studies follow similar distributions, with the majority of OSNs expressing zero or one δ-Pcdh. In contrast, the NanoString dataset detects more δ-Pcdhs per cell. Ribbons represent standard deviation following repeated bootstrapping of samples.
(L) Mean number of δ-Pcdhs per OSN from single cell RNA-seq datasets and NanoString. Numbers above bars represent the number of *Ncam1* positive cells in each study.

219   **δ-Pcdhs Are Homophilic Cell Adhesion Molecules**
220   To determine how δ-Pcdh combinations affect adhesion, we used K562 cell aggregation
221   assays. K562 cells are commonly used to study adhesion mediated by cadherins
222   because it is believed they do not express endogenous cadherins and are non-adherent
223   (Ozawa and Kemler, 1998; Schreiner and Weiner, 2010; Thu et al., 2014)
224
225   Our initial experiments showed extracellular and transmembrane domain (ECTM)
226   constructs were easier to express than full-length constructs. Importantly, the ECTM
227   domain was sufficient to drive homophilic adhesion (Figure 2 - Supplement 1A). As our
228   goal was to isolate the effects of adhesion on cell-cell interactions, we chose to use the
229   ECTM domain for all subsequent experiments. As expected, the exogenously
230   expressed protocadherins localized to sites of intracellular contact (Figure 2 -
231   Supplement 1B). We also confirmed that δ-Pcdh adhesion is highly sensitive to EDTA,
232   consistent with being members of the calcium dependent cadherin superfamily (Figure 2
233   - Supplement 1C). Although all expressed δ-Pcdhs induced cell aggregation (Figure
234   2A), *Pcdh10* formed very small aggregates relative to the others. We titrated the amount
235   of DNA to try and normalize aggregate size (Figure 2B). However, varying the amount
236   of *Pcdh10* DNA had little impact on aggregate size. We therefore excluded *Pcdh10* from
237   further experiments.
238
239   We performed pair-wise assays by mixing cells expressing one δ-Pcdh (fused to P2A-
240   GFP) with those expressing another (fused to P2A-RFP). We found that cells
241   expressing the same δ-Pcdh intermix (Figure 2C, center diagonal) while cells
242   expressing different δ-Pcdhs segregate from one another. We interpret these results to
243   indicate that δ-Pcdh adhesion is strictly homophilic. Identical results were found for the
244   cPcdh subfamily using the same assay (Thu et al., 2014).
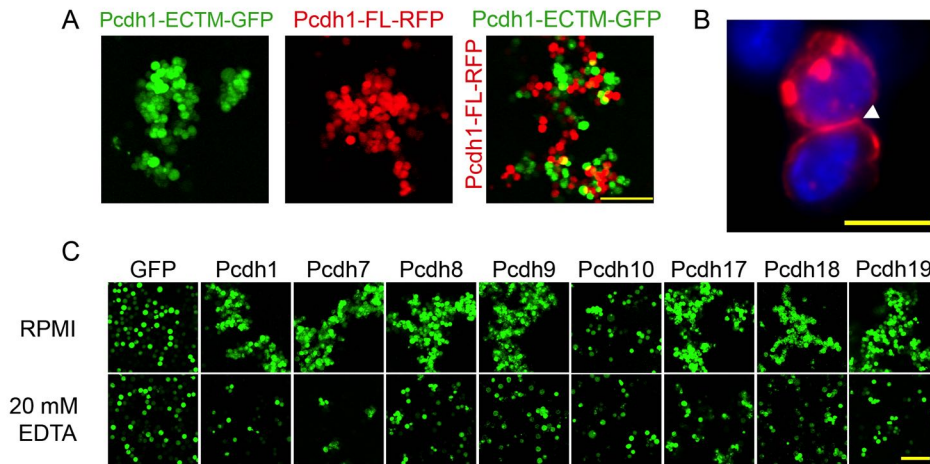
245　**Figure 2**
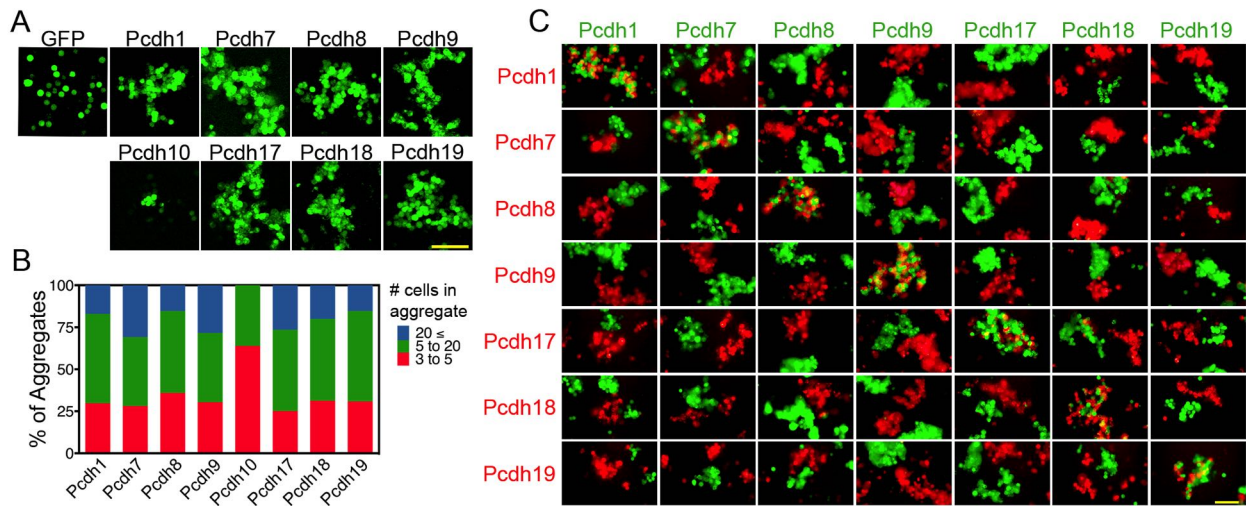
246
247

248　**Figure 2. δ-Pcdhs Mediate Homophilic Aggregation**
249　(A) Aggregates formed by ECTM constructs tagged with P2A-GFP. *Pcdh11x* could not
250　be expressed. Scale bar, 100 μm.
251　(B) Distribution of aggregate sizes after titrating DNA input. Results for each δ-Pcdh
252　were determined from three independent electroporations. *Pcdh10* aggregate size could
253　not be increased by varying DNA input.
254　(C) Pair wise analysis of δ-Pcdh binding specificity. Only pairs expressing the same δ-
255　Pcdh coaggregated (diagonal), while cells expressing different δ-Pcdhs segregated.
256　Results for each pair were determined from two independent electroporations. Scale
257　bar, 100 μm.

258 **Figure 2 – Supplement 1**

A Pcdh1-ECTM-GFP Pcdh1-FL-RFP Pcdh1-ECTM-GFP B

C GFP Pcdh1 Pcdh7 Pcdh8 Pcdh9 Pcdh10 Pcdh17 Pcdh18 Pcdh19

RPMI

20 mM
EDTA

259
260
261 **Figure 2 - Supplement 1. δ-Pcdh Homophilic Aggregation Does Not Require an**
262 **Intracellular Domain and is Sensitive to EDTA**
263 (A) Representative images of aggregates induced by a *Pcdh1* ECTM construct (left) and
264 a full length *Pcdh1* construct (middle). The two populations coaggregated when mixed
265 (right), demonstrating the intracellular domain is not required for homophilic recognition
266 and adhesion. Scale bar, 100 µm.
267 (B) δ-Pcdhs are localized at sites of intercellular adhesion (arrowhead). K562 cells
268 expressing *Pcdh7*-RFP were fixed and stained with DAPI prior to imaging. Scale bar, 10
269 µm.
270 (C) δ-Pcdh aggregation is severely disrupted by the presence of 20 µM EDTA, although
271 some δ-Pcdhs still maintained small aggregates (e.g. *Pcdh8* and *Pcdh17*). Scale bar,
272 100 µm.

Mismatch Coaggregation Assays Reveal Differences in Adhesion Among δ-Pcdhs

273 To determine how combinatorial expression of δ-Pcdhs affect adhesion specificity, we
274 next performed mismatch coaggregation assays. In these experiments, cells expressing
275 a single δ-Pcdh are mixed with a second population of cells expressing the same δ-
276 Pcdh plus an additional, "mismatched" δ-Pcdh. Prior studies on cPcdhs using this
277 approach showed that a single mismatch causes one population to segregate from the
278 other, even when several cPcdhs are expressed in common (Thu et al., 2014). In
279 contrast, this same assay suggested adhesive outcomes may be dependent on which δ-
280 Pcdhs were co-expressed (Pederick et al., 2018).
281
282
283 To systematically define how mismatched δ-Pcdhs influence adhesive outcomes, we
284 screened 42 possible mismatch pairs. We discovered a range of outcomes that could
285 be grouped into three broad categories (Figure 3A-D). In the first, the two populations
286 intermixed (Figure 3A,B). In the second, the populations interfaced (Figure 3C), and in
287 the last, the populations segregated from one another (Figure 3D). We also noticed that
288 interfacing and intermixing behaviors were not binary, but instead appeared to exist on
289 a continuum.
290
291 To better capture these differences, we developed a novel metric called the
292 CoAggregation Index (CoAg) to quantify the degree of coaggregation (see Methods).
293 Briefly, the index measures the proportion of red and green cells that share a common
294 boundary within a given confocal image. In general, CoAg values below 0.1 indicate
295 segregation, whereas values between 0.1-0.2 are typical of populations that interface.
296 Above 0.2, aggregates display increasingly higher degrees of intermixing. Thus, the
297 CoAg index captures subtle differences in aggregation behavior not easily identified by
298 eye. Ordering the CoAg values from our screen from high to low revealed a surprisingly
299 linear range of behavior (Figure 3E; mean CoAg values for a given experiment are
300 indicated in the corner of each representative image). For comparison, the first column
301 shows the CoAg value for *Pcdh1* cells mixed with *Pcdh7* cells (e.g. complete
302 segregation), as expected from cPcdh mismatch assays (Thu et al., 2014). The red bar
303 indicates complete mixing by matched populations.

303 Reordering the CoAg values into a heat map strongly argued that different δ-Pcdh
304 combinations produced different coaggregation behaviors (Figure 3F). For example, we
305 combined *Pcdh1* cells with cells expressing *Pcdh1+Pcdh7* or *Pcdh1+Pcdh8*. In the first
306 case, cells interfaced (CoAg=0.11; row 1, column 2), but in the second, they intermixed
307 (CoAg=0.27; row 1, column 3). Although *Pcdh1* was expressed by all populations, the
308 presence of *Pcdh7* vs. *Pcdh8* led to differing behaviors. This suggested that, unlike the
309 cPcdhs, the identity of the δ-Pcdh being tested is important for the outcome.

310 This is further reinforced by the fact that strong asymmetry is observed across the
311 diagonal in the heat map. For example, *Pcdh19* cells segregate from *Pcdh19+Pcdh7*
312 cells (CoAg=0.02; Figure 3G). However, "across the diagonal," *Pcdh7* cells intermix with
313 these same *Pcdh19+Pcdh7* cells (CoAg=0.40). Similarly, *Pcdh19* cells intermix with
314 *Pcdh19+Pcdh9* cells (CoAg=0.23) but across the diagonal, *Pcdh9* cells segregate
315 (CoAg=0.07). These results strongly suggest that coaggregation is dependent upon the

316 identity of the mismatched δ-Pcdh. We obtained similar results using full-length
317 constructs that could be expressed to generate an aggregation behavior (data not
318 shown). To compare how different δ-Pcdhs influence mismatch coaggregation, we
319 generated a net mismatch score that revealed a potential hierarchy among δ-Pcdhs
320 (Figure 3H, see Methods).

321 **Figure 3**

322
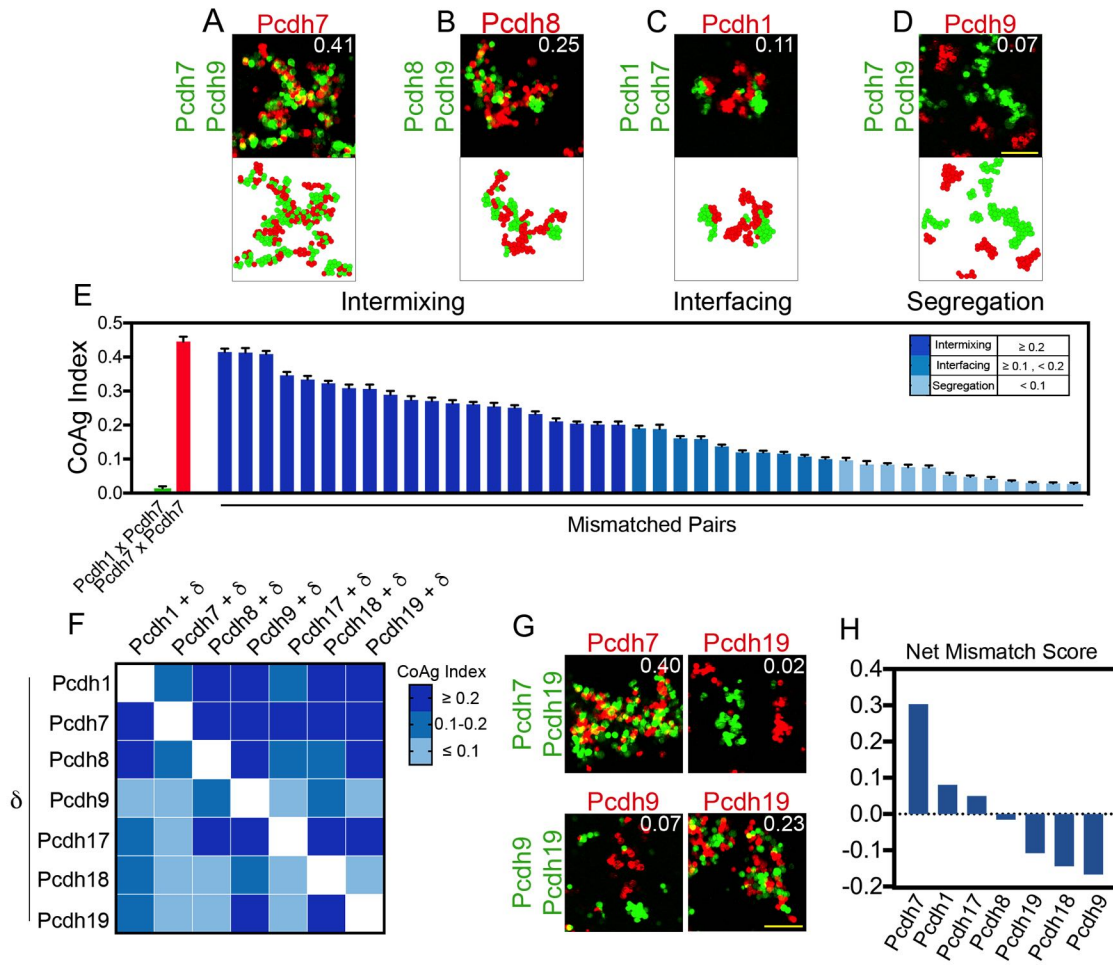
Figure 3. Mismatch Coaggregation Screen Reveals Complex Patterns of Differential Adhesion

(A-D) Representative examples of different coaggregation behaviors (mean CoAg values for each experiment are displayed in the upper right of each representative image). Examples of (A) high intermixing, (B) moderate intermixing, (C) interfacing, and (D) segregation behaviors. Scale bar, 100 µm.

(E) Range of coaggregation behaviors in our mismatch screen as revealed by the CoAg Index.

(F) Heat map of mean CoAg values from the screen reveals high asymmetry across the diagonal. Each row represents a population expressing a single δ-Pcdh, while each column represents the cells co-expressing the listed δ-Pcdh plus the corresponding row partner. White boxes indicate redundant homophilic pairs and were not tested. Results for each of the 42 pairs tested were determined from two independent electroporations.

(G) Examples of asymmetric behavior. *Pcdh7* cells intermix with *Pcdh7+Pcdh19* cells while *Pcdh19* cells segregate. *Pcdh19* cells intermix with *Pcdh9+Pcdh19* cells while *Pcdh9* cells segregate. Scale bar, 100 µm.

(H) Net mismatch scores estimate the ability of a given δ-Pcdh to overcome a mismatch and still coaggregate. *Pcdh7* has the highest such score and Pcdh9 the lowest, illustrating a potential hierarchy among δ-Pcdhs.
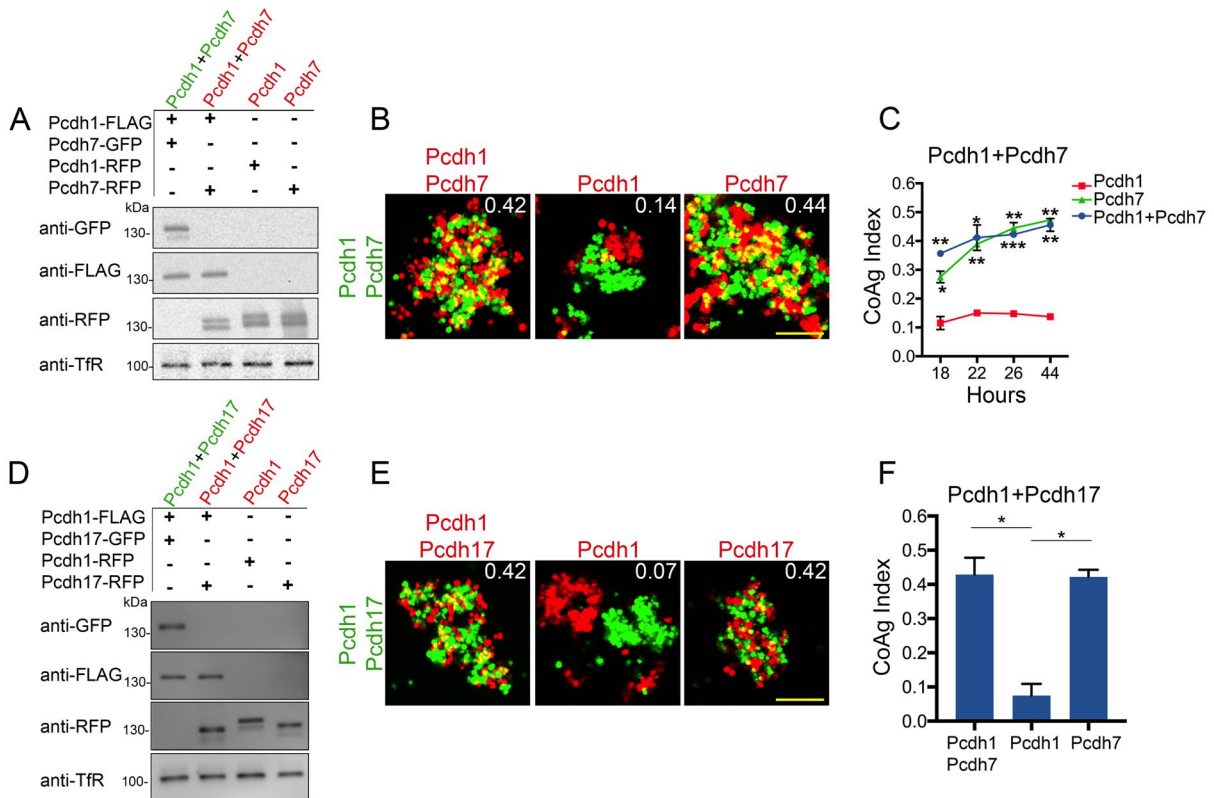
Differential Mismatch Coaggregation Outcomes Persist After Normalizing Surface Expression

We next considered if these variable behaviors were caused by differential surface expression of co-expressed δ-Pcdhs. Some prior studies control for overall expression (e.g. from whole cell lysates), but not surface expression. To address this, we generated ECTM constructs fused to FLAG, GFP, or RFP, and used a cell-impermeant biotinylation reagent to label surface protein in live cells. Labeled proteins were then affinity purified and analyzed by Western blotting for the various tags (Figure 4 - Supplement 1A). Antibody signal intensities were calibrated to allow for cross-antibody comparisons.

We re-tested all possible combinations of *Pcdh1*, *Pcdh7*, and *Pcdh17*, as these three had the strongest net mismatch scores in our initial screen (Figure 3H). For *Pcdh1+Pcdh7* mismatch assays, we controlled for surface expression by carefully titrating DNA input (Figure 4A), and examined aggregation behavior at 18, 22, 26, and 44 hours post electroporation. As seen in our initial screen, *Pcdh7* cells intermixed with *Pcdh1+Pcdh7* cells across all time points, whereas *Pcdh1* cells interfaced (Figure 4B,C). We used 26 hours for all further tests, given no obvious differences in behavior beyond this point.

We repeated the assay for *Pcdh1+Pcdh17*, and found that *Pcdh1* cells segregated (CoAg=0.07, Figure 4D-F), while *Pcdh17* cells intermixed (CoAg=0.42). Interestingly, these results differ from our preliminary screen, where both *Pcdh1* and *Pcdh17* cells interfaced with *Pcdh1+Pcdh17* cells. These results argue that controlling for surface level is important for interpreting coaggregation behavior, an aspect we explore below. Finally, we repeated our mismatch assay with *Pcdh7* and *Pcdh17*. We again found differences in behavior (Figure 4 – Supplement 1B-D). However, we found that this pair was particularly sensitive to DNA input, as small changes could alter the result despite minor effects on surface expression (Figure 4 - Supplement 1D). For one DNA input condition, *Pcdh17* cells interfaced (CoAg=0.29), while in the other they segregated (CoAg=0.08). In contrast, *Pcdh7* cells shifted towards intermixing. Nevertheless, these results confirm that differences in aggregation are dependent on δ-Pcdh identity.

Finally, we titrated surface expression for cells co-expressing *Pcdh1+Pcdh7+Pcdh17* (Figure 4 - Supplement 1E). We tested all 3 vs 1 (Figure 4 - Supplement 1F), 3 vs 2 (Figure 4 - Supplement 1G) and 2 vs 2 (Figure 4 - Supplement 1H) mismatch combinations. Differential adhesive behaviors were maintained as combinatorial depth increased, with the coaggregation outcome depending on which δ-Pcdhs were present (Figure 4 - Supplement 1I).

379 **Figure 4**

380
381 **Figure 4. Differential Coaggregation Outcomes Persist After Controlling for**
382 **Surface Expression Levels**
383 (A) Western blot of biotinylated membrane protein showing all populations in a
384 *Pcdh1+Pcdh7* mismatch assay possess similar surface expression levels after titration.
385 (B) Representative images from the mismatch assay at 26 hours. *Pcdh1* cells interface
386 with *Pcdh1+Pcdh7* cells while *Pcdh7* cells intermix. Scale bar, 100 µm.
387 (C) Mean CoAg values for each population at each time point. Each p-value is with
388 respect to *Pcdh1*. Error bars indicate ± SEM, * indicates p ≤ 0.05, ** p ≤ 0.01, *** p ≤
389 0.001. Results for each assay were determined from two independent electroporations.
390 (D) Western blot of biotinylated membranes showing all populations in a *Pcdh1+Pcdh17*
391 mismatch assay possess similar levels of surface expression after titration.
392 (E) Representative images from the *Pcdh1+Pcdh17* mismatch assay at 26 hours. *Pcdh1*
393 cells segregate while *Pcdh17* cells intermix. Scale bar, 100 µm.
394 (F) Mean CoAg values at 26 hours post electroporation. Error bars indicate ± SEM, *
395 indicates p ≤ 0.05. Results for each assay were determined from three independent
396 electroporations.

Figure 4 – Supplement 1
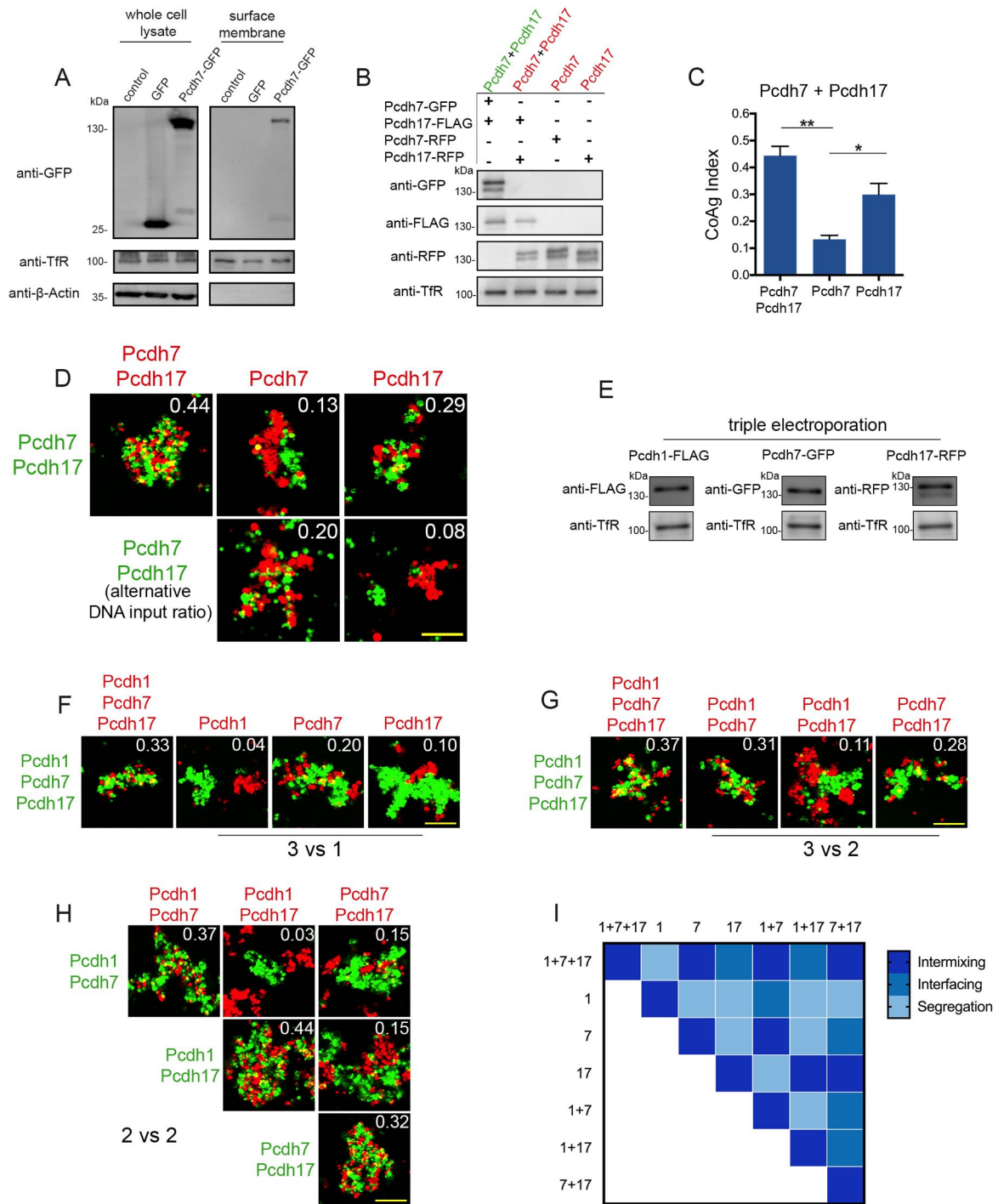
399 **Figure 4 - Supplement 1. Differences Among δ-Pcdhs in Coaggregation Behavior**
400 **Remain Despite Controlling for Surface Expression Levels**
401 (A) Western blot comparing whole cell lysate (left panel) with membrane fractions
402 following surface biotinylation (right panel). Surface membrane samples show no
403 detectable signal for cytosolic GFP or beta-actin, but are enriched for the surface
404 membrane marker transferrin receptor (TfR). The difference in expression of *Pcdh7-*
405 GFP in the whole cell lysate vs. the surface membrane sample highlights the
406 importance of measuring surface expression.
407 (B) Western blot of biotinylated membrane protein showing all populations in a
408 *Pcdh7+Pcdh17* mismatch assay possess similar levels of surface expression.
409 (C) Mean CoAg values for each population. Error bars indicate ± SEM, * indicates p ≤
410 0.05, ** indicates p ≤ 0.01. Results for each assay were determined from three
411 independent electroporations.
412 (D) Representative images of *Pcdh7+Pcdh17* mismatch assay. Note that the mean
413 CoAg values for *Pcdh7* and *Pcdh17* can be shifted with minor variations in DNA input
414 ratios. Such sensitivity was not observed for any other pair tested. Scale bar, 100 µm.
415 (E) Western blot of biotinylated membrane protein showing all populations in a
416 *Pcdh1+Pcdh7+Pcdh17* mismatch assay possess similar levels of surface expression.
417 For imaging experiments, tags were interchanged to prevent color mixing within a single
418 population.
419 (F) 3 vs 1 mismatch assays using *Pcdh1+Pdh7+Pcdh17* cells. *Pcdh1* cells segregated,
420 *Pcdh17* cells interfaced, while *Pcdh7* cells weakly intermixed. Scale bar, 100 µm.
421 Results for each assay were determined from three independent electroporations.
422 (G) 3 vs 2 mismatch assays using Pcdh1+*Pcdh7+Pcdh17* cells. *Pcdh1+Pcdh7* cells
423 intermix, *Pcdh1+Pcdh17* cells interface, and *Pcdh7+Pcdh17* cells intermix. Scale bar,
424 100 µm. Results for each assay were determined from three independent
425 electroporations.
426 (H) 2 vs 2 mismatch assays. Segregation, interfacing, and intermixing are observed
427 depending on the particular δ-Pcdhs expressed. Scale bar, 100 µm. Results for each
428 assay were determined from three independent electroporations.
429 (I) Heat map of mean CoAg outcomes for all *Pcdh1*, *Pcdh7* and *Pcdh17* combinations.

Coaggregation Behaviors Can be Modulated by Altering Relative Surface
Expression Levels

Our results argue that controlling for surface expression is important for understanding and interpreting differences in δ-Pcdh coaggregation behavior. In addition, our expression data (Figure 1A,B and Figure 1 - Supplement 1A-G) suggest that δ-Pcdh expression levels vary both within and between neurons. To further explore the role of expression, we established conditions where gradients of low, medium and high surface levels for *Pcdh1*, *Pcdh7*, and *Pcdh17* could be reproducibly generated (Figure 5A and Figure 5 - Supplement 1A). Medium levels were similar to those used in Figure 4.

Our mismatch assays involve mixing cells that express a single δ-Pcdh with those expressing two or more. We first asked what would happen if we altered surface expression in cells expressing a single δ-Pcdh. We found that *Pcdh1* (low, medium, and high) cells all still interfaced with *Pcdh1+Pcdh7* cells (Figure 5B,C), while *Pcdh7* (low, medium, and high) cells all still intermixed (Figure 5 - Supplement 1B,C). We found identical results with a different pair of δ-Pcdhs (Figure 5 - Supplement 1D-G). While the CoAg index varied slightly, the category of coaggregation behavior (intermix, interface, or segregation) did not. Thus, differences in mismatch coaggregation among δ-Pcdhs cannot be primarily explained based on variable expression in cells expressing one δ-Pcdh.

We next asked if altering the relative proportion of δ-Pcdh expression within cells expressing two δ-Pcdhs would affect coaggregation. We created populations with high and low DNA input values for each δ-Pcdh (e.g. $Pcdh1^{High}+Pcdh7^{Low}$ and $Pcdh1^{Low}+Pcdh7^{High}$ cells). We note that our goal was to simply alter the relative proportion of surface expression in these cells, and not to establish conditions where one δ-Pcdh was necessarily higher in expression than another. We found that varying the ratio of expression clearly altered coaggregation outcomes (Figure 5D,E).

Differences in coaggregation behavior are most easily seen by comparing results column by column. For example, in Figure 5D (column 1), *Pcdh1* cells intermix with $Pcdh1^{High}+Pcdh7^{Low}$ cells, but segregate from $Pcdh1^{Low}+Pcdh7^{High}$ cells. The coaggregation behavior of *Pcdh1* cells is therefore clearly affected by the ratio of *Pcdh1*:*Pcdh7* in the co-expressing cells. In the complementary experiment (column 2), *Pcdh7* cells intermixed with both $Pcdh1^{High}+Pcdh7^{Low}$ and $Pcdh1^{Low}+Pcdh7^{High}$ cells. However, intermixing was clearly reduced in $Pcdh1^{High}+Pcdh7^{Low}$ cells.

In column 3, $Pcdh1^{High}+Pcdh7^{Low}$ cells intermixed with $Pcdh1^{High}+Pcdh7^{Low}$ cells, but less well with $Pcdh1^{Low}+Pcdh7^{High}$ cells. The converse (column 4) was observed for $Pcdh1^{Low}+Pcdh7^{High}$ cells. Thus, relative surface levels of co-expressed δ-Pcdhs can influence aggregation behavior, even when there are no mismatches between populations.

We tested eight additional pairs using this high/low DNA input approach, and found similar results (Figure 5 - Supplement 1H). We confirmed a relative difference between high and low surface expression for a subset of pairs (Figure 5 - Supplement 1I). We conclude that changing the relative ratio of expression in cells expressing two δ-Pcdhs

472   has a much greater effect on coaggregation than varying expression in cells expressing
473   one δ-Pcdh.
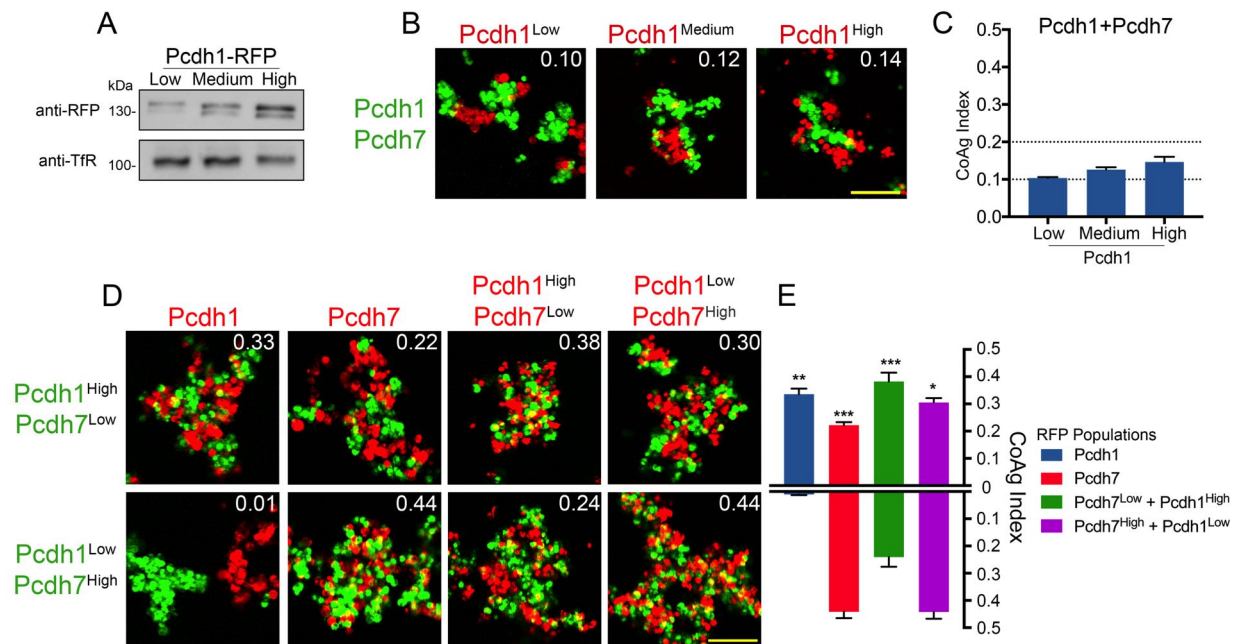
Figure 5

476   **Figure 5. Relative Surface Expression Modulates Mismatch Coaggregation**
477   **Behavior**
478   (A) Western blot of biotinylated membranes showing low, medium, and high surface
479   expressing populations of *Pcdh1* after DNA titration.
480   (B) Representative images of mismatch coaggregation assays mixing *Pcdh1*+*Pcdh7*
481   cells with *Pcdh1* (low, medium, and high) cells. Scale bar, 100 μm. Results for each
482   assay were determined from three independent electroporations.
483   (C) Mean CoAg values show varying the expression levels in *Pcdh1* cells did not alter
484   the coaggregation behavior (interfacing), but did affect the degree of interfacing. Error
485   bars indicate ± SEM. Dotted lines indicates thresholds for change in coaggregation
486   category.
487   (D) Representative images of mismatch coaggregation assays where the relative
488   expression levels of co-expressed δ-Pcdhs were varied. *Pcdh1*^{High}+*Pcdh7*^{Low} cells and
489   their complement, *Pcdh1*^{Low}+*Pcdh7*^{High} cells, were combined with cells expressing a
490   given δ-Pcdh population. The two images in a given column (e.g. *Pcdh1*, column 1)
491   illustrate the differences in coaggregation behavior when mixed with these two
492   populations.
493   (E) Mean CoAg values for (D), each bar indicates values for the top image in a given
494   column vs. values for the lower image in a given column. Error bars indicate ± SEM, *
495   indicates p ≤ 0.05, ** p ≤ 0.01, *** p ≤ 0.001. Results for each assay were determined
496   from four independent electroporations.

Figure 5 – Supplement 1

A

Pcdh7-RFP

| kDa | Low | Medium | High |

anti-RFP 130-

anti-TfR 100-

Pcdh17-RFP

| kDa | Low | Medium | High |

130-

100-

B

Pcdh7^{Low} Pcdh7^{Medium} Pcdh7^{High}

0.32 0.40 0.42

Pcdh1 Pcdh7

C

Pcdh1+Pcdh7

CoAg Index

Low Medium High

Pcdh7

D

Pcdh1^{Low} Pcdh1^{Medium} Pcdh1^{High}

0.04 0.05 0.06

Pcdh1 Pcdh17

E

Pcdh1+Pcdh17

CoAg Index

** * *

Low Medium High

Pcdh1

F

Pcdh17^{Low} Pcdh17^{Medium} Pcdh17^{High}

0.37 0.40 0.42

Pcdh1 Pcdh17

G

Pcdh1+Pcdh17

CoAg Index

Low Medium High

Pcdh17

H

I
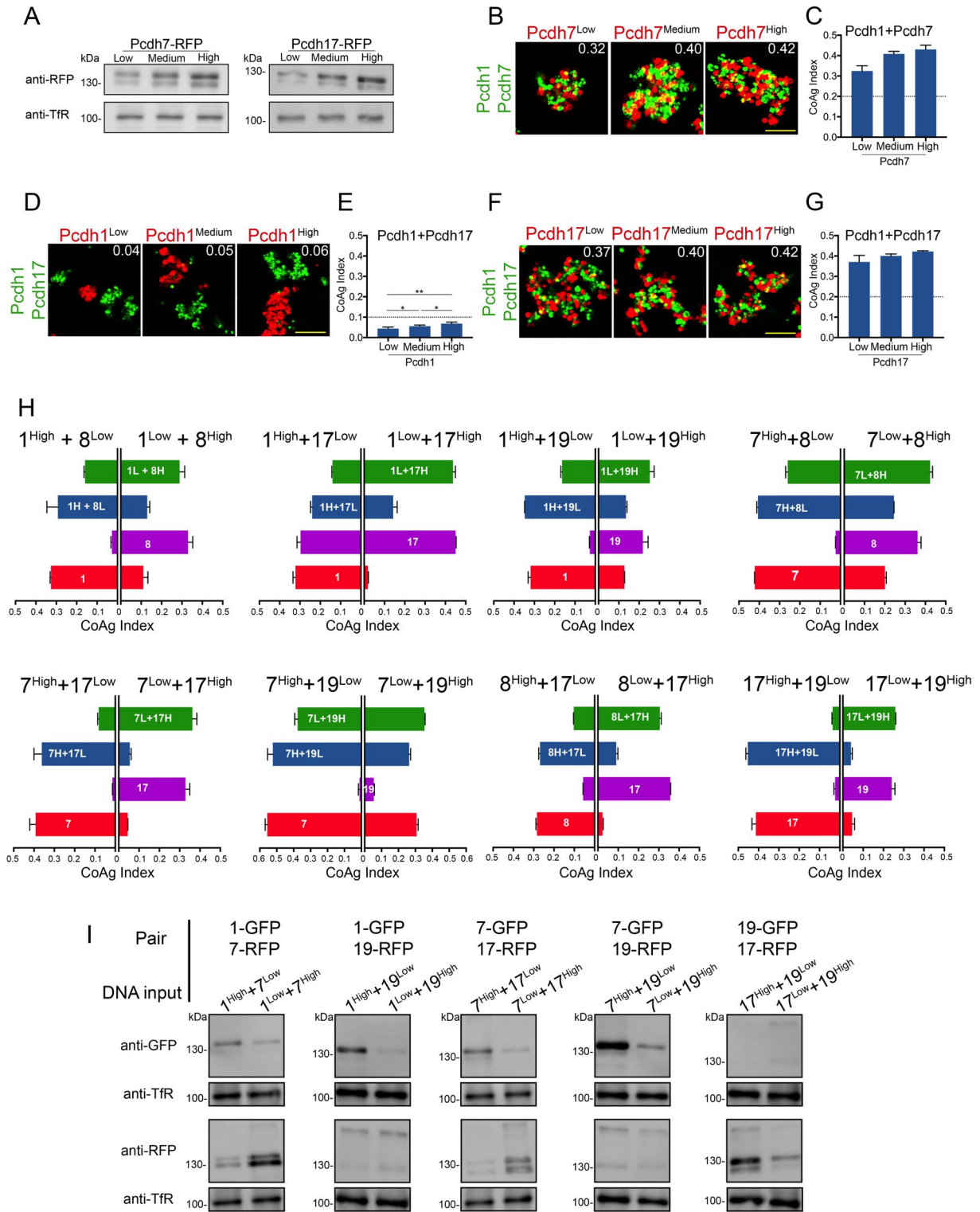
Figure 5 - Supplement 1. Effects of Surface Expression Levels on Mismatch Coaggregation Behavior

(A) Western blots of purified membranes showing low, medium, and high levels of *Pcdh7* and *Pcdh17* surface expression after DNA titration.

(B,D,F) Representative images of mismatch coaggregation assays with (B) *Pcdh1+Pcdh7* and (D,F) *Pcdh1+Pcdh17* cells.

(C,E,G) Mean CoAg values show varying surface expression in cells expressing a single δ-Pcdh did not fundamentally alter coaggregation behavior. Dotted lines indicate the threshold to change coaggregation categories. Cells still intermixed (*Pcdh7, Pcdh17*) or segregated (*Pcdh1*), although small changes in CoAg values do occur with increasing expression. Error bars indicate ± SEM, * indicates p ≤ 0.05, ** p ≤ 0.01. Results for each assay were determined from three independent electroporations.

(H) The impact of changing relative expression levels in cells expressing two δ-Pcdhs was tested for eight additional pairs of δ-Pcdhs. Each graph shows the mean CoAg values obtained for each mismatch assay. For example, the first graph shows the effects of varying relative expression of *Pcdh1+Pcdh8*. The left half of this graph shows results from assays using $Pcdh1^{High}+Pcdh8^{Low}$ cells, while the right half shows results using the opposite conditions ($Pcdh1^{Low}+Pcdh8^{High}$). The impact of changing these relative expression levels is easiest to interpret by comparing the left and right half of each horizontal bar. For example, for the first bar (green), $Pcdh1^{Low}+Pcdh8^{High}$ cells intermix more strongly with cells expressing $Pcdh1^{Low}+Pcdh8^{High}$ than with $Pcdh1^{High}+Pcdh8^{Low}$ cells. *Pcdh8* cells (purple bar) intermixed with $Pcdh1^{Low}+Pcdh8^{High}$ cells, but segregated from $Pcdh1^{High}+Pcdh8^{Low}$ cells. Changing the relative level of expression in co-expressing cells can therefore change the category of coaggregation behavior. Error bars indicate ± SEM. Results for each assay were determined from two independent electroporations.

(I) A subset of conditions shown in (H) and in Figure 5D were tested to confirm high/low DNA inputs resulted in changes in relative surface expression. Compare relative signal from the top half of each lane to the bottom. Note that the goal was to generate different expression ratios between the two lanes for each pair shown, and not to generate "high" or "low" surface expression.

δ-Pcdhs Possess Different Apparent Adhesive Affinities

530

531 Because differences in δ-Pcdh coaggregation behavior persisted despite controlling for
532 surface expression, we next asked whether they possess differences in apparent
533 adhesive affinity. Such differences have been argued to mediate segregation among
534 classical cadherins, such as *N-* and *E-cadherin* (Harrison et al., 2010; Katsamba et al.,
535 2009). We hypothesized that we could detect these potential differences by subjecting
536 aggregates to higher shear forces. Cells expressing δ-Pcdhs with weaker apparent
537 adhesive affinities should dissociate prior to those expressing δ-Pcdhs with stronger
538 affinities.

539

540 We generated cells expressing *Pcdh1*, *Pcdh7* or *Pcdh17* at high surface levels (Figure
541 5A, S4A), and subjected them to gradual increases in rotational speed (15-220 RPM).
542 Images were analyzed for aggregate size using a custom written code (Aggregate Size
543 Measurement). Three populations began dissociating as speed increased. However,
544 *Pcdh7* cells maintained larger aggregates than *Pcdh1* or *Pcdh17* cells at all speeds
545 (Figure 6A,B). Furthermore, while *Pcdh1* and *Pcdh17* cells appeared to fully dissociate
546 by ~200 RPM, *Pcdh7* aggregates were still present even at 220 RPM. Because *Pcdh1*,
547 *Pcdh7*, and *Pcdh17* were at one end of our hierarchy (Figure 3H), we compared *Pcdh1*
548 and *Pcdh19* using the same approach. Similarly, we found that *Pcdh1* cells maintained
549 larger aggregates than *Pcdh19* cells at all speeds (Figure 6 - Supplement 1A-C).

550 Varying expression levels also accentuated these differences. We generated cells
551 expressing *Pcdh7* or *Pcdh17* at low, medium and high levels (Figure 5A and Figure 5 –
552 Supplement 1A). As expected, we found that higher surface levels generated larger
553 aggregates that could better withstand increasing rotational speeds (Figure 6 -
554 Supplement 1D-G). We also found that *Pcdh7* cells produced larger aggregates at all
555 speeds compared to *Pcdh17* cells. Even at 220 RPM, *Pcdh7*[Low] cells still maintained
556 some aggregates.

557 If *Pcdh1* has weaker apparent adhesive affinity than *Pcdh7*, this difference could explain
558 why *Pcdh1* cells interface with *Pcdh1+Pcdh7* cells while *Pcdh7* cells intermix in
559 mismatch assays. Such differences should be accentuated by increasing shear force on
560 aggregates. To test this, we repeated the *Pcdh1+Pcdh7* mismatch assay. After allowing
561 aggregates to form at 15 RPM, we increased the speed to 120 RPM. Despite the
562 increased speed, *Pcdh7* cells still intermixed with *Pcdh1+Pcdh7* cells. However, *Pcdh1*
563 cells now segregated (Figure 6C,D), consistent with weaker apparent adhesive affinity.

564 To examine structural differences that could account for this varying behavior among δ-
565 Pcdhs, we performed multiple sequence comparison by log expectation (MUSCLE)
566 alignments. We found low sequence identity among δ-Pcdhs in extracellular domains
567 (EC) 1-4 (~35%; Figure 6 - Supplement 1H). Prior work had shown that the adhesive
568 interface of *Pcdh19* was localized to EC1-4 (Cooper et al., 2016). To test the
569 importance of EC1-4 in adhesion mediated by other subfamily members, we deleted
570 these domains (Δ1-4) from *Pcdh1*, *Pcdh7* and *Pcdh17*. Although the truncated proteins
571 were still transported to the surface, they were unable to mediate adhesion (Figure 6 -

572 Supplement 1I,J). To determine how EC1-4 affect mismatch coaggregation, we mixed
573 cells co-expressing *Pcdh1+Pcdh7*$^{\Delta1\text{-}4}$ with those expressing *Pcdh1* or *Pcdh7* alone.
574 *Pcdh7* cells could no longer intermix, and switched to a segregation behavior
575 (CoAg=0.01; Figure 6 - Supplement 2A,B). Conversely, *Pcdh1* cells switched from
576 interfacing to intermixing (CoAg=0.25). Next, we swapped the EC1-4 of *Pcdh7* with that
577 from *Pcdh1* (*Pcdh7*$^{EC1\text{-}4:Pcdh1}$). These cells now intermixed with *Pcdh1* cells, but
578 segregated from *Pcdh7* cells (Figure 6 - Supplement 2C,D, column 3). Finally, *Pcdh1*
579 cells now intermixed with *Pcdh7*$^{EC1\text{-}4:Pcdh1}$*+Pcdh1* cells, while *Pcdh7* cells segregated
580 (Figure 6 - Supplement 2C,D; column 4). These results are consistent with EC1-4
581 mediating adhesive specificity.

582 Our results argue that differences in apparent adhesive affinity and relative surface
583 expression regulate coaggregation behavior. We therefore performed Monte Carlo
584 simulations using a custom program (cellAggregator) to see if we could model these
585 factors *in silico*. We successfully captured the behavior of a subset of our experiments.
586 The model functioned most optimally in predicting cells that will intermix. For example,
587 the model correctly predicted that cells expressing identical δ-Pcdhs will intermix.
588 Furthermore, the model also predicted the behavior of cells known to intermix in
589 mismatch coaggregation assays. However, the model could not precisely recapitulate
590 conditions where cells interfaced or segregated (Figure 6E, far right column; e.g. mixing
591 *Pcdh1* cells with *Pcdh1+Pcdh7* cells). Varying affinity differences, relative expression
592 levels, or both still did not completely capture these behaviors. We anticipate other, as
593 yet uncharacterized effects (e.g. intracellular δ-Pcdh-δ-Pcdh interactions (Pederick et
594 al., 2018)) must be incorporated into the model to better capture cell adhesive behavior.
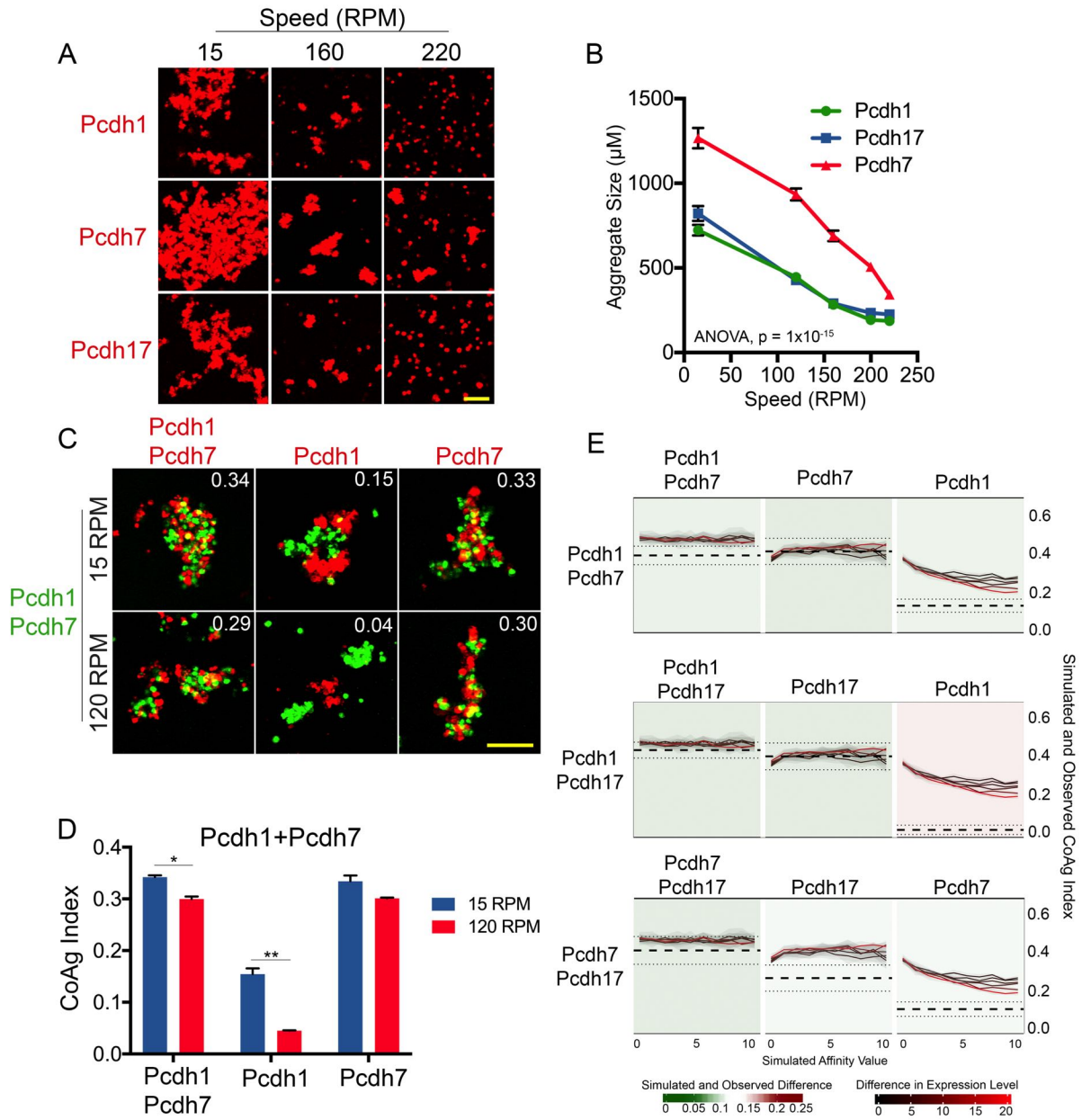
595   **Figure 6**

596

Figure 6. δ-Pcdhs Possess Differences in Apparent Adhesive Affinity

(A) Representative images of cell aggregates at select speeds. *Pcdh7* cells possessed small aggregates even at 220 RPM while *Pcdh1* and *Pcdh17* cells dissociated. Scale bar, 100 μm.

(B) Mean aggregate size at each speed. *Pcdh1* and *Pcdh17* were significantly different from *Pcdh7* by ANOVA, $p=1\times10^{-15}$. Error bars indicate ± SEM. Results for each assay were determined from four independent electroporations.

(C) Representative images of a mismatch coaggregation assay with *Pcdh1+Pcdh7* cells. At higher speeds, *Pcdh1* cells change from interfacing to segregating (middle column), while the other two populations remain intermixed. Scale bar, 100 μm.

(D) Mean CoAg values of (C). Error bars indicate ± SEM, * indicates $p \leq 0.05$, ** indicates $p \leq 0.01$. Results for each assay were determined from three independent electroporations.

(E) Monte Carlo simulations incorporating affinity and relative expression level capture most, but not all, mismatch assay results. We modeled the behavior of a given mismatch assay (e.g. row 1, *Pcdh1+Pcdh7*). The Y-axis represents the CoAg Index (simulated (solid black and red lines) and observed (thick dashed line with standard error represented by thin dashed lines)). Solid lines represent simulations where the relative expression level of the two δ-Pcdhs has been varied (from 1:1 to 20:1). The X-axis represents increasing differences in apparent adhesive affinity (e.g. the left most point on the X-axis represents conditions where both δ-Pcdhs are of equal apparent adhesive affinity). In all three simulated coaggregation assays, the model predicted intermixing conditions (e.g. CoAg index above 0.2), but was not able to precisely model segregation or interfacing behaviors (compare right most graph in each row against the other two).

Figure 6 – Supplement 1
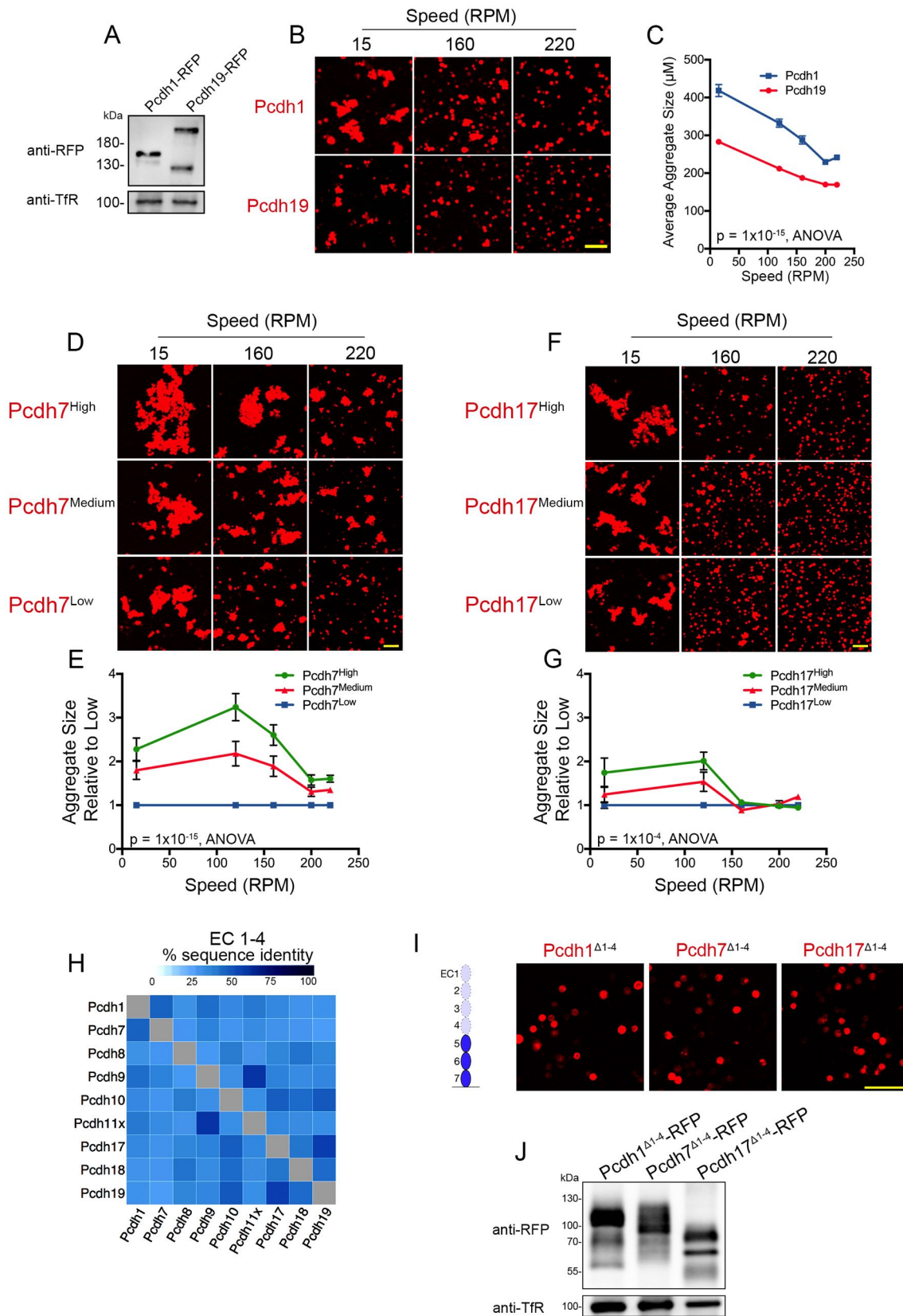
624 **Figure 6 - Supplement 1. δ-Pcdhs Possess Differences in Apparent Adhesive**
625 **Affinity, Which Appears to be Mediated by EC Domains 1-4**
626 (A) Western blot showing similar surface level expression for *Pcdh1* and *Pcdh19* cells.
627 A second, high-molecular weight band is frequently observed for *Pcdh19*.
628 (B) Representative images of cell aggregates taken at various speeds. Scale bar, 100
629 µm.
630 (C) Quantification of aggregate size shows *Pcdh1* cells maintained larger aggregates
631 than *Pcdh19* cells at all speeds. *Pcdh1* and *Pcdh19* cell behaviors were significantly
632 different by ANOVA, p = 1×10^{-15}. Error bars indicate ± SEM. Results for each assay
633 were determined from four independent electroporations.
634 (D-G) Cells expressing high, medium, and low levels of *Pcdh7* (D) and *Pcdh17* (F) were
635 subject to increasing rotational speeds. Mean aggregate sizes for *Pcdh7* (E) and
636 *Pcdh17* (G). Increased surface expression led to larger aggregates at each speed
637 tested. Error bars indicate ± SEM. Results for each assay were determined from three
638 independent electroporations.
639 (H) MUSCLE protein alignments show low overall sequence identities for EC1-4.
640 (I) *Pcdh1$^{\Delta1-4}$*, *Pcdh7$^{\Delta1-4}$* and *Pcdh17$^{\Delta1-4}$* constructs fail to mediate adhesion. Cartoon
641 illustrates EC1-4 deletion for *Pcdh1* and *Pcdh7*. *Pcdh17* construct has only two EC
642 domains following deletion of EC1-4. Scale bar, 100 µm.
643 (J) Western blot of biotinylated surface show proteins with deletions in EC1-4 are
644 transported to the surface.
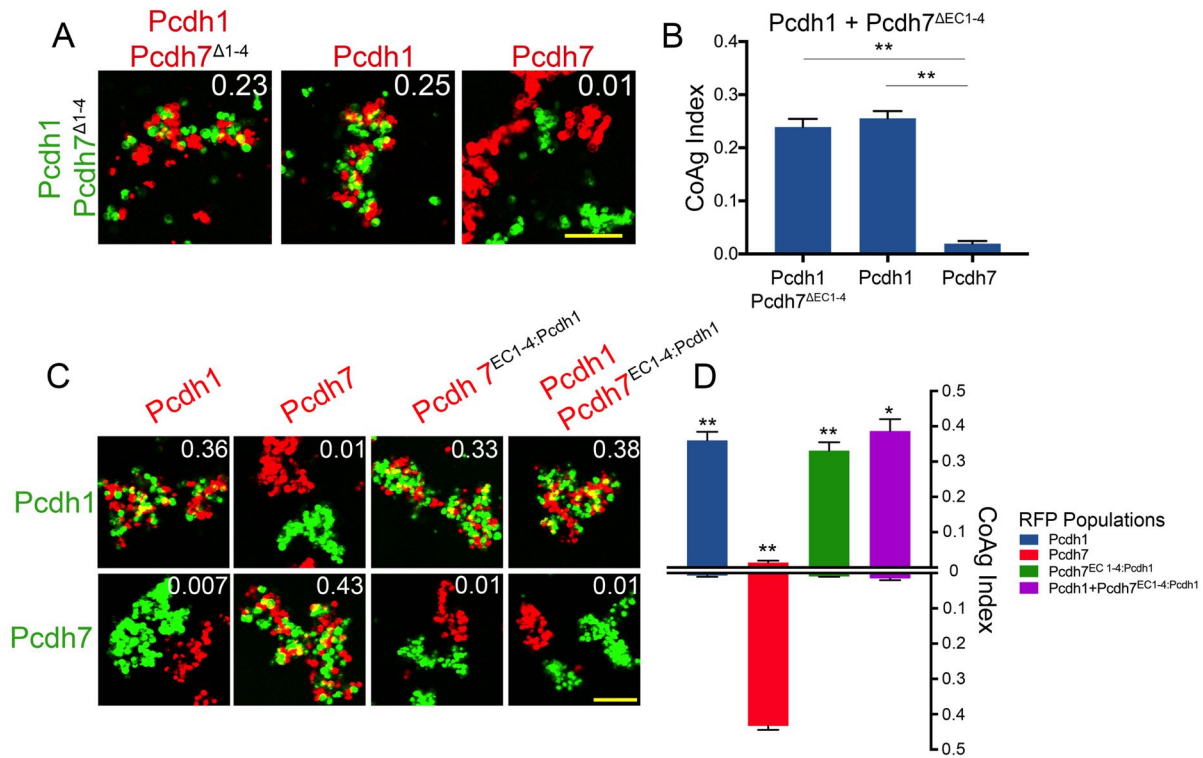
Figure 6 – Supplement 2

Figure 6 - Supplement 2. EC1-4 Mediate Adhesive Interactions among δ-Pcdhs
(A) Representative images of coaggregation assay with *Pcdh1+ Pcdh7$^{\Delta1-4}$* cells. *Pcdh1*
cells now intermix with this population while *Pcdh7* cells segregate. Scale bar, 100 μm.
(B) Mean CoAg values, error bars indicate ± SEM, * indicates p ≤ 0.05, ** indicates p ≤
0.01 Results for each assay were determined from three independent electroporations.
(C) Representative images of coaggregation assay where EC1-4 of *Pcdh7* has been
swapped with that from *Pcdh1*. Results are best interpreted by comparing images within
individual columns. Columns 3 and 4 shows the swap construct *Pcdh7$^{EC1-4:Pcdh1}$* enables
these cells to now intermix with *Pcdh1* cells, and cause *Pcdh7* cells to now segregate.
Scale bar, 100 μm.
(D) Mean CoAg values. Values from the top half of each bar should be compared
against those in the bottom half to visualize differences in coaggregation behavior. Error
bars indicate ± SEM, * indicates p ≤ 0.05, ** indicates p ≤ 0.01. Results for each assay
were determined from three independent electroporations.

Increasing Combinatorial δ-Pcdh Expression and Interactions With a cPcdh Family Member

Our single cell RNA analysis showed individual OSNs express up to seven δ-Pcdhs. To test the impact of increasing the number of co-expressed δ-Pcdhs on mismatch aggregation, we generated populations of cells that co-expressed *Pcdh7* with one to four additional δ-Pcdhs. To confirm changes in the relative expression of *Pcdh7* vs the other co-expressed δ-Pcdhs, we measured surface expression levels (Figure 7A) and performed coaggregation assays with cells expressing only *Pcdh7*. We found that each additional δ-Pcdh co-expressed with *Pcdh7* led to a corresponding decrease in the CoAg index (Figure 7B). *Pcdh7* only cells shifted from intermixing towards interfacing as the relative proportion of *Pcdh7* decreased. Quantification of surface expression showed that the percent of *Pcdh7* with respect to total surface expression decreased from ~50 to 25%, almost perfectly mirroring the decline in CoAg index (R^2=0.94; Figure 7C). We repeated the experiment with *Pcdh1*, and found a similar effect (Figure 7 - Supplement 1A,B). In this case, increasing the number of co-expressed δ-Pcdhs shifted the behavior of *Pcdh1* cells from interfacing to segregation.

Finally, although we have focused on how δ-Pcdh subfamily members function in combination, individual neurons are likely to co-express multiple cadherin subfamily members. How δ-Pcdhs and these other subfamily members interact is not well understood. We first confirmed that cPcdh *Pcdhb11* cells completely segregate from cells expressing δ-Pcdhs, demonstrating strict homophilic adhesion (Figure 7 - Supplement 1C). We then co-expressed *Pcdhb11* with *Pcdh7* in a mismatch coaggregation assay. We then generated populations co-expressing *Pcdh7* and *Pcdhb11* at three different relative levels (Figure 7D). At the first two (DNA input ratio of 3:4 and 1:2), surface levels of *Pcdh7* were ~45% of total (Figure 7E). Under these conditions, *Pcdh7* cells strongly intermixed while *Pcdhb11* cells segregated (Figure 7F,G). However, at a DNA ratio of 1:4 (*Pcdh7* ~20% of total), *Pcdh7* cells still intermixed but *Pcdhb11* cells could now interface. Thus, δ-Pcdhs influence the aggregation behavior of cells expressing this particular cPcdh. This raises the intriguing possibility that the two subfamilies may work in concert to specify adhesion.

692   **Figure 7**
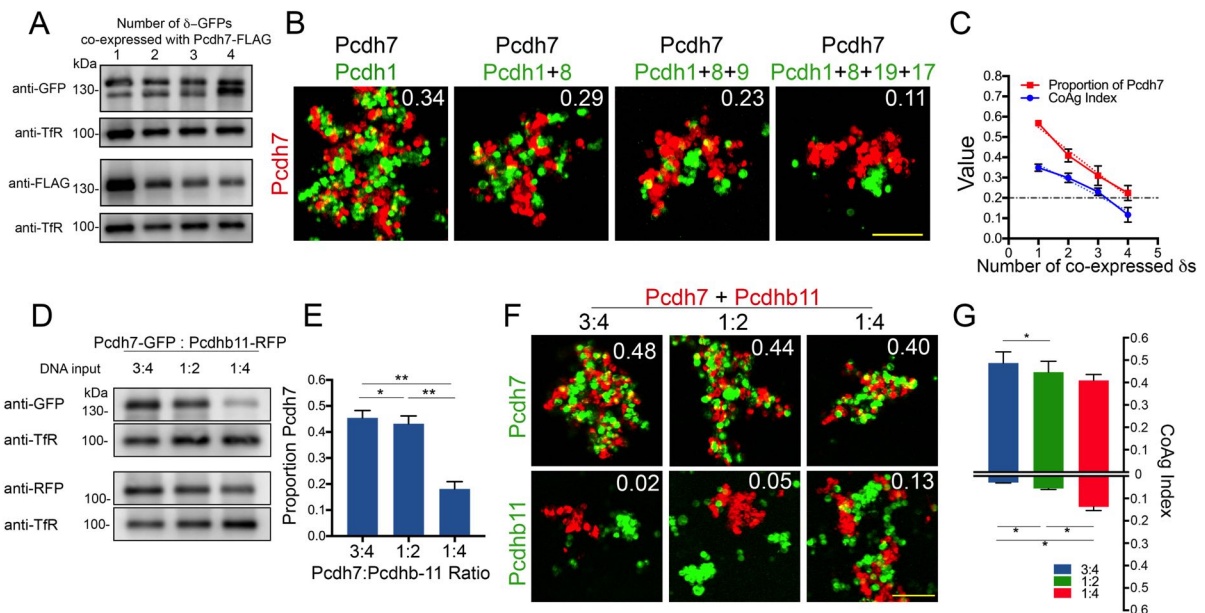
693
694   **Figure 7. Effect of increasing co-expression of δ-Pcdhs on adhesion and**
695   **interactions with cPcdh b11**
696   (A) Western blot showing surface expression of *Pcdh7* (FLAG) in the presence of
697   increasing numbers of co-expressed δ-Pcdhs (all labeled with GFP).
698   (B) Representative images of *Pcdh7* cells when mixed with *Pcdh7*+increasing numbers
699   of δ-Pcdhs. Note shift from intermixing (left panel) to interfacing (right panel) as the
700   number of δ-Pcdhs increases. Scale bar, 100 μm.
701   (C) Linear regression analysis of mean CoAg values (R^2=0.94; blue) and relative
702   surface expression of *Pcdh7* (red) with increasing numbers of co-expressed δ-Pcdhs.
703   Error bars indicate ± SEM. Results for each assay were determined from three
704   independent electroporations. Dot-dash line indicates boundary between intermixing
705   and interfacing. R^2 = 0.97 and 0.98 for CoAg index and proportion of *Pcdh7* on surface,
706   respectively.
707   (D) Western blot of *Pcdh7* and *Pcdhb11* surface expression with varying DNA input
708   ratios.
709   (E) Quantitation of western blot data shown in (D). Error bars indicate ± SEM. Results
710   for each assay were determined from three independent electroporations.
711   (F) Representative images and (G) Mean CoAg values of coaggregation assays with
712   *Pcdh7*+*Pcdhb11* cells. As the ratio of *Pcdh7*:*Pcdhb11* decreases, the CoAg value of
713   *Pcdhb11* cells increases, and shifts from segregation to interfacing (compare bars on
714   bottom half of graph). Although the CoAg values of *Pcdh7* drop somewhat (compare
715   bars on top half of graph), *Pcdh7* cells still intermix, despite low DNA input ratios. Error
716   bars indicate ± SEM, * indicates p ≤ 0.05. Results for each assay were determined from
717   three independent electroporations. Scale bar, 100 μm.

Figure 7 – Supplement 1

A

B

C
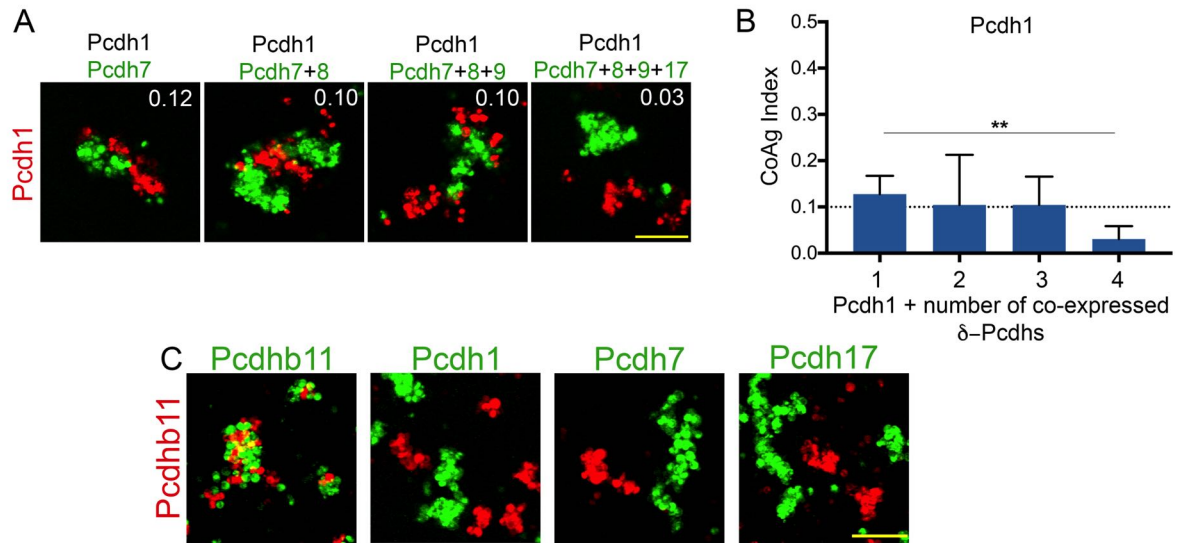
719

720 **Figure 7 - Supplement 1. Increasing δ-Pcdh Combinatorial Expression and**
721 **Homophilic Adhesion Among Protocadherins**
722 (A) Representative images of *Pcdh1* cells mixed with *Pcdh1*+increasing numbers of δ-
723 Pcdhs. Note cells shift from interfacing (left panel) to segregation (right panel) as the
724 number of δ-Pcdhs increases. Scale bar, 100 μm
725 (B) Mean CoAg index values fall as the number of δ-Pcdhs increases, and shifts
726 categories (e.g. drops below 0.1, the boundary between interfacing and segregation as
727 indicated by dotted line). Error bars indicate ± SEM, ** indicates p ≤ 0.01. Results for
728 each assay were determined from three independent electroporations.
729 (C) Representative images showing *Pcdhb11* will intermix with other *Pcdhb11* cells, but
730 will segregate from cells expressing a given δ-Pcdh. Scale bar, 100 μm.

Discussion

Our results provide a foundation for understanding how a small gene family can exert unexpectedly complex influences on cell adhesion. Despite the apparent range of combinatorial expression observed within single neurons, we identified two simple principles that dictate intrafamily interactions. First, we found individual δ-Pcdhs possess differences in apparent adhesive affinity. Second, these differences can be modulated by varying surface expression levels. Together, these principles dramatically augment the range of adhesive interactions mediated by this small subfamily. Despite the fact that there are only a limited number of δ-Pcdhs, these principles provide cells with the ability to carefully fine tune their adhesive profiles. Even if cells express the same combination of δ-Pcdhs, varying the levels of each expressed family member provides additional flexibility in modulating adhesion. These principles contrast with those defined for the cPcdhs. However, our results also provide an initial glimpse into how these two families can interact with one another to affect adhesion.

Differences in Apparent Adhesive Affinity Among δ-Pcdhs

The range of apparent adhesive affinities suggest that neurons can fine tune their overall adhesive profile by varying the repertoire of δ-Pcdhs expressed. One caveat is that we did not directly measure affinity using purified proteins. As our efforts are aimed at understanding how δ-Pcdhs mediate cell-cell interactions, we utilize the term apparent adhesive affinity to describe the functional impact of δ-Pcdhs on adhesion. Biophysical studies will be required to fully define such affinity differences. However, structural studies show cPcdhs possess varying adhesive affinities (Goodman et al., 2016; Rubinstein et al., 2015). Despite this, such differences do not appear to have a major impact in K562 assays (Thu et al., 2014).

While cell aggregation assays have been used for decades, the technical details have never been standardized. For example, cell type, speed of rotation, time of mixing, surface expression, and mode of quantitation all differ among past studies. We note that very few studies control for or report these factors, which in our hands are important for reproducible adhesive behavior. While such controls may not be necessary when cells essentially completely segregate from one another (e.g. as for cPcdhs), such reproducibility was essential to our ability to identify and quantitate differences in adhesive outcomes among δ-Pcdh family members.

Our aggregation assay results clearly contrast with a prior study of cPcdhs (Thu et al., 2014). In this paper, two populations would only fully intermix if they expressed the same combinations of cPcdhs. If even one cPcdh differed between the two, the populations would completely segregate, regardless of the identity of the mismatched cPcdh. The observed results were always binary in nature, and produced either complete intermixing or complete segregation. In contrast, we were able to observe a range of coaggregation behaviors. This spectrum of adhesive outcomes illustrates how a comparatively small gene family can still have complex effects on cellular behavior. Biophysical analysis of complex formation may better illuminate the mechanism behind such differences.

777 We note we did not identify any obvious differences between members of the δ-1 and δ-
778 2 subfamilies in our assays. Members of both groups were expressed in overlapping
779 patterns within the epithelium (Figure 1 – Supplement 1). *In situ* hybridization,
780 NanoString, and qRT-PCR analyses also showed no obvious differences between
781 subfamilies (Figure 1). In our mismatch aggregation assays, δ-1 and δ-2 members were
782 distributed along the spectrum of our net mismatch score (Figure 3). For example,
783 *Pcdh1*, a δ-1 family member, had a roughly equivalent net mismatch score with *Pcdh17*,
784 a δ-2 family member. However, we note that δ-1 and δ-2 members are often co-
785 expressed within neurons, leading to potential intracellular interactions that may not be
786 captured in these assays. Further, how the varying number of extracellular domains
787 between the two subfamilies influences adhesion is not known. Further structural
788 studies will be needed to better define how these differences affect cell-cell interactions.
789
790 **δ-Pcdh Adhesion Can Be Tuned by Varying Relative Expression Level**
791 We showed a simple solution to moderating high apparent adhesive affinity δ-Pcdhs is
792 to vary relative expression level. These results are reminiscent of principles defined for
793 classical cadherins. Steinberg's differential adhesion hypothesis provides a commonly
794 used framework for understanding how classical cadherins mediate cell sorting. In this
795 model, cells sort from one another to reach an optimal thermodynamic equilibrium. This
796 sorting can be driven by differences in adhesive affinity between cells, and/or by
797 differences in expression level (Foty and Steinberg, 2005; Friedlander et al., 1989;
798 Steinberg and Takeichi, 1994). Thus, δ-Pcdhs appear to use some of the same
799 principles as classical cadherins. However, Steinberg and colleagues typically focused
800 on N- and/or E-cadherin, and did not, to our knowledge, examine the behavior of
801 multiple classical cadherins in combination. The principles we define here therefore
802 confirm similarities between the classical and δ-Pcdhs, and extend these canonical
803 studies of cadherin function.
804
805 We chose to use the ECTM domain for these experiments because expressing the full-
806 length construct in K562 cells proved practically difficult. However, we demonstrated
807 that the ECTM domain mediated homophilic adhesion to a degree similar to that of the
808 full-length construct (Figure 2 - Supplement 1). As our goal was to study adhesive
809 interactions among co-expressed family members, this allowed us to separate adhesion
810 from intracellular signaling. Further, K562 cells are non-neuronal, and are unlikely to
811 replicate signaling within neurons. In addition, the ECTM domain is typically used to
812 study δ-Pcdh adhesion (Chen et al., 2007; Cooper et al., 2016; Emond et al., 2011).
813 Nevertheless, there are many aspects of δ-Pcdh function that are not addressed by this
814 reductionist approach. Intracellular signaling events, heterologous extracellular
815 interactions, and regulation of δ-Pcdh gene expression can all further tune the impact of
816 δ-Pcdhs on cell-cell interactions. Indeed, our Monte Carlo simulation indicates we can
817 capture many, but not all, behaviors associated with combinatorial expression. Most
818 notably, not all interface or segregation behaviors could be adequately modeled (Figure
819 6E). We expect that other, uncharacterized intracellular or extracellular interactions may
820 explain these differences. In particular, Pederick et al. showed δ-Pcdh*s* can interact in
821 *cis* (Pederick et al., 2018). Such *cis* interactions have previously been proposed to be
822 critical for cPcdh function (Rubinstein et al., 2017; Thu et al., 2014). If these *cis*

823   interactions are also important for δ-Pcdh function, we anticipate that they may
824   contribute towards adhesion of δ-Pcdhs in *trans*.

825

826   Nevertheless, our studies lay the foundation for new models that can integrate these
827   principles with those defined for other cadherin subfamilies, ultimately leading to a more
828   complete determination of cadherin function within the nervous system. Our results
829   represent a functional genomic approach towards understanding how combinations of
830   cadherin expression identified via transcriptomic approaches impact cellular function.

831

832   **Implications for δ-Pcdh Function *In Vivo***
833   Our reductionist approach to understanding δ-Pcdh function has the fundamental
834   advantage of allowing us to systematically test different combinations for their impact on
835   adhesion. Such studies would be extremely difficult to execute *in vivo*, given the varied
836   chromosomal locations of δ-Pcdhs and the technical complexity of manipulating multiple
837   genes at once. Further, although K562 cells have been used extensively to study
838   protocadherin function, they are not a neuronally derived line. An appropriate question
839   would be to ask how our result apply towards understanding δ-Pcdh function i*n vivo*.

840

841   We believe there are two major applications of this study for understanding δ-Pcdh
842   function. First, while δ-Pcdhs have been suspected to be expressed in combination *in*
843   *vivo* based on double-label RNA *in situ* data*,* there has been no prior evidence
844   demonstrating the extent of this expression. Our single cell NanoString and qRT-PCR
845   data (Figure 1D-F) clearly demonstrate that multiple δ-Pcdhs are expressed per neuron,
846   and show the variety and extent of such expression. Our round-robin RNA *in situ*
847   hybridization studies (Figure 1 – Supplement 1H) are also consistent with this
848   combinatorial expression. Further, our study of δ-Pcdh and odorant receptor overlap
849   showed OSNs known to project to different targets clearly express different proportions
850   of δ-Pcdhs (Figure 1B). While the expression of δ-Pcdh vs. a given odorant receptor is
851   not a simple, one-to-one correlation, there nevertheless were clear differences among
852   OSNs expressing different odorant receptors. Thus, the combinatorial expression of δ-
853   Pcdhs is not an entirely random event, as has been suggested for the cPcdhs
854   (Goodman et al., 2016; Hirano et al., 2012). This is further supported by our single label
855   RNA *in situ* studies, which clearly shows spatially restricted expression of δ-Pcdhs
856   within the olfactory epithelium (Figure 1 - Supplement 1B-G). Our results therefore
857   demonstrate that δ-Pcdhs are combinatorially expressed *in vivo,* that 0-7 family
858   members can be co-expressed within OSNs, and that this expression pattern is not
859   stochastic.

860

861   Second, our studies addressed the question of how these combinations could influence
862   δ-Pcdh function. Our results argue that the particular combination expressed within a
863   cell has a major impact on its adhesive profile. We therefore predict mutations in any
864   one δ-Pcdh will not have uniform effects on all cells that express that particular δ-Pcdh,
865   simply because different cells are likely to express different combinations. For example,
866   we previously showed that mis- and over-expression of *Pcdh10* in the olfactory system
867   caused defects in glomerular target formation by OSNs expressing the *Olfr9* odorant

868 receptor, but not by those expressing *Olfr17* (Williams et al., 2011). A recently
869 generated *Pcdh19* mutant mouse in our lab also shows targeting defects of a subset of
870 OSN populations (data not shown). If *Pcdh10* and *Pcdh19* are expressed by multiple
871 OSN populations (Figure 1B), why are only a subset of OSNs affected in these
872 mutants?
873
874 We speculate that this variation is due in part to the interactions between the mutated δ-
875 Pcdh and the other, co-expressed δ-Pcdhs within a neuron. Furthermore, the two
876 populations may express different levels of *Pcdh19,* leading to different effects when
877 *Pcdh19* is mutated. *A* true understanding of how mutations in δ-Pcdhs mediate their
878 effects would therefore be dependent on defining at a minimum what other δ-Pcdhs are
879 co-expressed within affected cells. Loss of any one δ-Pcdh would alter the combination
880 of δ-Pcdhs expressed and change the relative expression of co-expressed
881 protocadherins. The changes that would occur as a result of these intrafamily
882 interactions would therefore vary based on what δ-Pcdhs were co-expressed within the
883 cell.
884
885 This same K562 assay was used to examine a mouse mutant of *Pcdh19* to understand
886 why apparent cell sorting defects occurred in the cortex (Pederick et al., 2018).
887 Critically, this study postulated that co-expressed δ-Pcdhs might influence the observed
888 sorting behavior. They found that K562 cell adhesion was indeed affected by different δ-
889 Pcdh combinations. These studies did not correct for surface expression, or draw any
890 particular conclusions about principles that mediate their observed phenotypes.
891 Nevertheless, their results are consistent with ours in demonstrating the importance of
892 combinations in mediating cell sorting.
893
894 Our results therefore emphasize the importance of understanding what combinations
895 exist within neurons in order to understand observed phenotypes. However, defining the
896 particular combination of δ-Pcdhs expressed per neuron has been problematic. Single
897 cell RNA-seq studies have been unable to adequately address what combinations are
898 expressed within individual neurons. Our own analysis of three single OSN RNA-seq
899 datasets (Hanchate et al., 2015; Saraiva et al., 2015; Tan et al., 2015) shows an
900 average detection of ~1 δ-Pcdh per neuron, while our NanoString approach detects
901 ~3.5 (Figure 1 - Supplement 1K,L). Furthermore, our NanoString results were consistent
902 with orthogonal validation assays using qRT-PCR and *in situ* hybridization. Thus, higher
903 sensitivity approaches, similar to those used here, may be necessary to fully address
904 what combinations are present within neurons.
905
906 We would also like to highlight the importance of potential, interfamily interactions. We
907 demonstrated co-expression of *Pcdh7* with *Pcdhb11* inhibits *Pcdhb11* from intermixing
908 with *Pcdh7+Pcdhb11* cells (Figure 7F,G). If, however, expression of *Pcdh7* is reduced
909 relative to *Pcdhb11*, then these cells begin to display interfacing behavior. Thus, δ-
910 Pcdhs can modify the behavior of other, co-expressed subfamily members. It seems
911 reasonable that δ-Pcdhs, classical cadherins, cPcdhs, and other subfamily members are
912 all likely to be co-expressed within individual neurons. How would interfamily
913 interactions influence neuronal behavior *in vivo*?

914   Studies on cPcdhs have emphasized the sheer number of possible stochastic
915   combinations that can be generated with this family. Our studies demonstrate that even
916   greater adhesive complexity can be generated by superimposing the effects of δ-Pcdhs
917   on cells expressing cPcdhs. Although we and others have begun establishing rules
918   governing intrafamily interactions, it is likely that further complexity can be added via
919   interactions between subfamilies. For example, δ-Pcdhs can bind and regulate classical
920   cadherins (Chen and Gumbiner, 2006; Chen et al., 2009; Emond et al., 2011).. Such
921   interfamily interactions may well help to explain certain mutant phenotypes associated
922   with the cPcdhs. In the retina, deletion of cPcdhs leads to neuronal death and to defects
923   in dendritic self-avoidance. Interestingly, interactions between cPcdh subfamilies
924   accentuates these effects (Ing-Esteves et al., 2018), again underscoring the impact of
925   combinatorial subfamily interactions. However, in the cortex, deletion of cPcdhs disrupts
926   dendritic branching due to a failure to promote arborization (Molumby et al., 2016).
927   Thus, the same family has distinct effects in different regions of the nervous system.
928   These differences were proposed to be due to context dependent effects. However, it is
929   conceivable that interfamily interactions, such as those between the δ-Pcdhs and the
930   cPcdhs, may also play a role in explaining these varying phenotypes. The fundamental
931   principles defined here therefore enable new hypotheses to be generated regarding
932   how mutations in protocadherins influence neuronal function.

Key Resources Table				
Reagent type (species) or resource	**Designation**	**Source or reference**	**Identifiers**	**Additional information**
gene (Mus musculus)	Pcdh1	this paper	NM_029357.3	cloned from isolated RNA from mouse olfactory epithelium
gene (Mus musculus)	Pcdh7	this paper	AB006758.1	cloned from isolated RNA from mouse olfactory epithelium
gene (Mus musculus)	Pcdh8	this paper	NM_001042726.3	cloned from isolated RNA from mouse olfactory epithelium
gene (Mus musculus)	Pcdh9	this paper	NM_001271798.1	cloned from isolated RNA from mouse olfactory epithelium
gene (Mus musculus)	Pcdh10	this paper	NM_001098172.1	cloned from isolated RNA from mouse olfactory epithelium
gene (Mus musculus)	Pcdh11x	this paper	XM_006528392.3	cloned from isolated RNA from mouse olfactory epithelium
gene (Mus musculus)	Pcdh17	this paper	XM_006518905.2	cloned from isolated RNA from mouse olfactory epithelium
gene (Mus musculus)	Pcdh18	this paper	XM_006500789.2	cloned from isolated RNA from mouse olfactory epithelium
gene (Mus musculus)	Pcdh19	this paper	NM_001105246.1	cloned from isolated RNA from mouse olfactory epithelium
strain, strain background (Mus musculus)	FVB/NJ	The Jackson Laboratory	1800	
strain, strain background (Mus musculus)	C57BL/6J	The Jackson Laboratory	664	
strain, strain background (Mus musculus)	CD-1	Charles River	22	
genetic reagent ()				
cell line (Homo sapiens)	K-562	ATCC	CCL-243	
transfected construct ()				
transfected construct ()				
biological sample (Mus musculus)	primary olfactory sensory neurons	this paper		isolated for single cell analysis from P6-P8 mice, both sexes
biological sample (Mus musculus)	olfactory epithelium	this paper		isolated and sectioned for RNA *in situ* hybridization, at ages indicated in paper, both sexes
antibody	moust anti-GFP	Thermo Scientific	MA5-15256	1:4,000
antibody	mouse anti-RFP	Thermo Scientific	MA5-15257	1:2,000
antibody	mouse anti-FLAG	Thermo Scientific	MA1-91878	1:6,000
antibody	mouse anti-Transferrin Receptor (TfR)	Thermo Scientific	13-6800	1:1,000
recombinant DNA reagent	N1-p2a-GFP or RFP	this paper		modified from Clontech N1-eGFP
recombinant DNA reagent	N1-GFP or RFP	this paper		modified from Clontech N1-eGFP
sequence-based reagent		this paper		see supplemental tables for all primers
peptide, recombinant protein				
commercial assay or kit	Pierce Cell Surface Isolation Kit	Thermo Scientific	89881	

commercial assay or kit	Ingenio Electroporation Kit	Mirus	MIR 50118	
chemical compound, drug	Valproic acid sodium salt	Sigma-Aldrich	P4543	4 µM
software, algorithm	Co-Ag index	this paper		code written in Mathematica (Wolfram Research)
software, algorithm	Aggregate size measurement	this paper		code written in Mathematica (Wolfram Research)
software, algorithm	Cell aggregation Monte Carlo Simulator	this paper		https://github.com/shazanfar/cellAggregator

934

Methods

Animal Use
All animal protocols were approved by the Cornell Institutional Animal Care and Use Committee. Non-Swiss Albino (NSA) mice of mixed sex were used for all single cell studies. For RNA *in situ* hybridization experiments, both NSA and C57Bl/6 mice were used. Mice were sacrificed at post-natal day 7 (P7) for single cell and single label RNA *in situ* hybridization experiments, and embryonic day 17.5 (E17.5) for double label experiments.

RNA *In Situ* Hybridization and Quantification
Single and double label RNA *in situ* hybridization was performed essentially as described (Williams et al., 2011). For single color studies at E17.5 and P7, at least three independent heads were analyzed. For δ-Pcdh co-expression studies, three replicates were performed from three different heads for each gene. Imaging of double-label RNA i*n situ* data was performed using a Leica (Wetzlar, Germany) LSM 510 confocal microscope, and multiple locations within each E17.5 olfactory epithelia were examined. Five optical slices (each 3 µm thick) from each location were used to assess co-expression. Positive co-expression was manually determined based on overlapping fluorescence signal observed in consecutive optical sections. Between 71 and 167 cells were analyzed per double label comparison. To quantify single label RNA *in situ* data, slides were scanned with a ScanScope (Leica) using a 20x objective. The OSN layer of each section was manually traced using HALO software (Indica Labs, Corrales, New Mexico), and the percent positive area was determined using a built-in software module. For δ-Pcdh and odorant receptor co-expression studies, an average of 70 OSNs expressing a given odorant receptor were analyzed for co-expression with any one δ-Pcdh.

Single OSN Isolation
Olfactory epithelia were dissected from P7 NSA mice and enzymatically dissociated for one hour using the Papain Dissociation Kit (Worthington, Lakewood, NJ). The tissue was manually triturated, and the papain neutralized as per manufacturer's instructions. Approximately 250,000 cells were then plated on coverslips coated with poly-ornithine, and the cells were allowed to recover at 37ºC with 6% CO_2 for 30 minutes in Modified Eagle's Medium (MEM). After recovery, the cells were gently washed three times with

969   CO$_2$ equilibrated MEM. The coverslip was then transferred to a 10 cm dish, where it was
970   immobilized by applying small dabs of autoclaved Vaseline between the bottom of the
971   coverslip and the 10 cm dish. The dish was flooded with 10 mL of equilibrated MEM,
972   and individual OSNs isolated by manual aspiration under a 20X objective using a
973   micromanipulator (Eppendorf; Hauppauge, New York). Micropipettes for aspiration were
974   prepared using a Sutter P-97 Flaming/Brown (Novato, CA) micropipette puller, and pre-
975   filled with ~3 μL of MEM. After aspiration, the contents were transferred to a PCR tube
976   by gently snapping the distal tip of the micropipette inside the tube and expelling the
977   contents using a needle and syringe. Two different lysis buffers were utilized (Cells-to-
978   Ct or CellsDirect, Thermo-Fisher, Waltham, MA), with no apparent difference in lysis
979   quality or NanoString results. Each tube was pre-loaded with 6 μL of CellsDirect lysis
980   buffer (containing lysis enhancer) or Cells-to-Ct buffer (containing DNAse I). As OSN
981   isolation was performed at room temperature, neurons were collected from a given
982   coverslip within 30 minutes. Cells processed in CellsDirect buffer were stored at -80ºC
983   until processing. Cells processed in Cells-to-Ct buffer were vortexed and then incubated
984   at room temperature for five minutes. An additional 0.5 μL of stop solution was added
985   and incubated for 2 minutes at room temperature before being stored at -80ºC until
986   further processing.
987
988   **Amplification and Quality Control of Single OSNs**
989   Amplification reactions were done using the CellsDirect kit (Thermo-Fisher) essentially
990   according to manufacturer's instructions, with the following modifications. The 31 gene
991   multiplex primer set was added to individual lysates (100 nM final, see Supplemental
992   File) in a final volume of 10 μL. Tubes were heated at 80ºC for 10 minutes and chilled
993   on ice for 3 minutes. 10 μL of 2x reaction buffer and 1 μL of SuperScript III/Platinum
994   Taq (Thermo-Fisher) were added and tubes were reacted in a PCR machine at 50ºC for
995   one hour, followed by 85ºC for 15 minutes to inactivate the reverse transcriptase. PCR
996   amplification was then performed with an initial activation at 94ºC for 2 minutes,
997   followed by 18 cycles of 94ºC for 30 seconds, 60ºC for 30 seconds, and 72ºC for 30
998   seconds. After amplification, 20 μL of 10mM Tris 7.5 was added to each sample to bring
999   up the total volume to 40 μL. Four μL of each sample was then screened by quantitative
1000 PCR to determine expression levels of *Gapdh* (indicating successful capture and
1001 amplification) and *Ncam1* (indicating an OSN). Taqman primers were designed to
1002 amplify regions internal to the 31 gene multiplex primer sequence, and samples were
1003 run on an ABI 7500 (Thermo-Fisher). Only cells with Ct values ≤ 25 for both genes were
1004 used for the NanoString analysis (Seattle, WA). See Supplemental File for primer
1005 sequences.
1006
1007 **NanoString nCounter Processing and Validation**
1008 A custom codeset of 31 genes was designed that would detect a select subset of known
1009 axon guidance genes (see Supplemental File). Single cell cDNA was hybridized to the
1010 codeset in collaboration with NanoString. Genes were determined to be positively
1011 expressed using a constrained gamma-normal mixture model approach (Ghazanfar et
1012 al., 2016). Briefly, 'negative' control genes (e.g. *Notch2*, *Gfap* and *Cdh13*) were used to
1013 estimate the distribution of the no or lowly expressed genes across all cells. Following
1014 this, for each cell a constrained gamma-normal mixture model was fit using the

1015 Expectation Maximization (EM) algorithm, constrained in the sense that the mean and
1016 variance of the no or lowly expressed component for that particular cell was the same
1017 as across all cells, allowing the highly expressed component to vary as required. This
1018 constrained gamma-normal mixture model allowed for 'sharing' of information across
1019 multiple cells, reducing the possibility of ill-fitting distributions to the cells' expression
1020 patterns. Following model fitting, cells and genes were classed as 'expressed' if the
1021 corresponding posterior probability was 0.5 or above, and 'not expressed' otherwise.
1022 After this analysis, some cells were found to be *Notch2* positive, and discarded from
1023 further study. Data from four codeset genes generated no useful information and were
1024 not utilized.
1025
1026 **Single cell qPCR validation**
1027 OSNs were isolated and amplified in a manner identical to those used for NanoString
1028 analysis. Two uL of amplified cDNA from each single cell were used as template for
1029 each Taqman assay (*Gapdh*, *Ncam1*, *Notch2*, and the δ-Pcdhs; Supplemental File 1).
1030 All primer sets displayed efficiencies between 93-100%, except for *Pcdh1* which had
1031 83% efficiency (improvement was not observed with multiple primer designs). Probes
1032 were designed to bind to regions distinct from those detected with the NanoString
1033 codeset. Genes were considered "on" if we observed a C_t value less than or equal to
1034 30.
1035
1036 **Plasmid Construction**
1037 EGFP-N1 (Clontech) vectors were modified to incorporate the TagRFP fluorophore
1038 and/or a P2A sequence. FLAG constructs were created in a pHAN vector modified to
1039 include a FLAG sequence at the 3' terminus of the polylinker. ECTM domains of δ-
1040 Pcdhs were then cloned into the appropriate vector.
1041
1042 **K562 Aggregation Assay**
1043 K562 cells were purchased from ATCC (ATCC CCL-243) and tested mycoplasma
1044 negative. Low passage number cells (4-10 passages) were maintained in RPMI + L-
1045 glutamine with 10% calf bovine serum (Gemini Bio, Sacramento, CA). Cells were grown
1046 to a density between 250-500,000 cells/mL prior to electroporation. For the
1047 electroporation, one million cells were removed, concentrated by centrifugation, and
1048 resuspended in 100 µL of Ingenio Electroporation Solution (Mirus Bio, Madison, WI).
1049 Five to eight µg of cesium chloride or midi prepped (Omega) DNA for each δ-Pcdh to be
1050 expressed was added, and the cells electroporated using an Amaxa Nucleofector II
1051 (Lonza; program T-016, Cologne, Germany). Cells were allowed to recover for one hour
1052 at 37ºC by immediate addition of 2 mLs of CO_2 equilibrated media. After recovering,
1053 valproic acid (VPA, 4mM final; Sigma, St. Louis, MO) was added to promote expression.
1054 Preliminary control experiments showed VPA did not affect cell adhesion, as cells
1055 electroporated with vector only remained non-adherent up to four days. For
1056 coaggregation experiments, equal volumes of cells from a given electroporation were
1057 mixed immediately following the recovery period and placed in individual wells of a 6-
1058 well (2 mLs/well) or 24-well (0.5 mLs/well) plate. Cells were gently and continuously
1059 agitated at 15 RPM overnight in a tissue culture incubator at 37ºC with 6% CO_2.
1060

Cell Aggregation Imaging

For initial aggregate size titration, 15-20 images were taken of each replicate using an inverted fluorescent microscope (Nikon, Tokyo, Japan) with a 10x objective. For speed and aggregate size experiments, ~6 field of views were captured at each speed for each replicate using a confocal microscope (Zeiss LSM 510) with a 5x objective. For all other aggregation experiments, ~10-15 confocal images were captured of each replicate using a 10x objective.

CoAggregation Index (CoAg)

To generate the Coaggregation Index, confocal images were analyzed using custom code ("CoAg") written in Mathematica (Wolfram Research, Champaign, IL). Briefly, each confocal image of an aggregate is parsed into squares just slightly larger than the area of a single cell. After removing all black squares from the image (those containing no cells), the remaining squares are analyzed to calculate the percent of squares that contain more than one color. As a result, cells that completely segregate from one another will have a very low CoAg index because few squares will contain more than one color. In contrast, cells that interface will have higher CoAg indices as green and red cells abut one another, while those that intermix will have the highest index.

Aggregate Size Titration Assay

K562 cells were electroporated and following a one hour recovery period, allowed to form aggregates at 15 RPM overnight. At 24-26 hours, images were captured of each replicate. To determine size of aggregates, images were analyzed using the particle size plugin in ImageJ. Aggregates smaller than three cells were removed from the analysis to prevent dividing cells and single cells not participating in aggregation from skewing the results. Aggregate pixel size was compared to the pixel area of one cell to approximate the number of cells per aggregate.

Speed Aggregation Assay

K562 cells were electroporated and following the 1 hour recovery period, allowed to form aggregates at 15 RPM overnight. At 24-26 hours, images were captured to establish a 15 RPM baseline. Plates were then returned to the incubator and the speed increased for 1 hour to 120 RPM. Images were then acquired, and this process repeated at 160, 200 and 220 RPM. Each image was then analyzed using a custom written code ("Aggregate Size Measurement") in Mathematica (Wolfram Research, Champaign, IL) to measure the pixel size of each aggregate, and aggregate pixel size was then converted to microns.

Statistical Analyses

For mismatch coaggregation assays, paired t-tests were performed between each paired population to determine statistical significance in Prism (Graph Pad, La Jolla, CA). For aggregate speed and size analyses, analysis of variance (ANOVA) were performed in R.

Biotinylation Assay

Surface biotinylation of live K562 cells was performed using the Pierce Cell Surface Isolation Kit (Thermo-Fisher) essentially as recommended. Volume of cell resuspension was reduced to 1 mL, and an additional 150 uL of lysis buffer was added to ensure complete mixing during incubation.

Western Blot Analysis

Western blots were performed by loading 8 uL (roughly 15% of the total elution from each biotinylation experiment) onto 10% SDS polyacrylamide gels. All primary antibodies used were monoclonal in origin, and carefully titrated to establish working dilutions of equivalent detection so that samples across antibodies could be compared. To achieve this, we calibrated working monoclonal concentrations with purified RFP and GFP proteins. We also electroporated cells with the same δ-Pcdh fused to different tags to optimize antibody dilution to account for variation in signal intensity. The antibodies used were mouse anti-GFP (1:4,000, Thermo-Fisher MA5-15256), mouse anti-RFP (1:2,000, Thermo-Fisher MA5-15257) and mouse anti-FLAG (1:6,000, Thermo-Fisher MA1-91878). We used the transferrin receptor (TfR) as a loading control for surface protein (1:1,000, Thermo-Fisher 13-6800). All antibodies were diluted in 20% glycerol upon receipt to promote cryostability. Estimation of band intensity was carried out using ImageJ.

Monte Carlo Simulation (cellAggregator)

To investigate the aggregation behavior of cell populations expressing δ-Pcdhs of varying apparent adhesive affinities and expression, we performed Monte Carlo based simulations to describe cell binding interactions as a dynamic cell-cell network across discrete time steps using custom code (cellAggregator). Two cell populations, green (n = 25) and red (n = 25), were assigned properties of two hypothetical genes named A and B, corresponding to the coaggregation assay experiments conducted. For example, green cells could be designated as expressing high levels of A and low levels of B, and red cells as expressing low levels of B and high levels of A. The genes A and B were each also assigned binding affinities, e.g. A possesses two times greater apparent adhesive affinity than B. The initial cell-cell network consists of the green and red cells as nodes in the network, and edges represent cell-cell binding interactions occurring.

For each simulation, 100 time steps were performed. At each discrete time point, the cells are mixed and allowed to bind to other cells according to a 'speed dating' set up, where the majority of cell pairs (arbitrarily set at 75%) result in a cell-cell interaction. Allowing the majority (as opposed to all cell pairs) to bind avoids oscillatory network behavior. The probability that two cells would 'speed date' increased as the Euclidean distance between the force-directed network projection onto two dimensions decreased, i.e. nodes more closely connected were more likely to 'speed date'. Once 'speed-dating' begins, the cell pair would bind via the genes expressed by each cell, with unbound genes selected at random with a probability corresponding to the expression level. The duration of interaction (number of time steps) depended on the identity of genes. A-B interactions persisted for only a single time step, while B-B interactions persisted for three time steps, and A-A interactions persisted for three multiplied by the affinity ratio time steps. This differential length of time for cell-cell interactions is based on the idea

1153 that non-homophilic protocadherin interactions are unstable and do not persist (A-B),
1154 and that some protocadherins may have different levels of apparent adhesive affinity,
1155 leading to more persistent or stable binding time (e.g. A-A lasts more time steps than B-
1156 B if A is assigned greater affinity than B). The green or red color of the cells did not
1157 affect the binding of cell pairs.

1158 Instantaneous network coaggregation was measured by calculating the average
1159 proportion of different-color to same-color binding partners across all cells in the
1160 network for any one time step. Cells with no network partners were not included in this
1161 calculation. The *in silico* coaggregation behavior for the entire simulation was then
1162 determined as an average of all instantaneous network coaggregations in the
1163 simulation. This value did not include initial time steps (arbitrarily set at 25% of the 100
1164 total time steps) to allow for the network to stabilize following the initial state of all cells
1165 being unconnected. This resulted in a single overall *in silico* coaggregation index value
1166 determined for the simulation scenario. A total of 100 time steps were simulated for
1167 each scenario, and each scenario was repeated five times. To model varying affinity
1168 between genes, the affinity values were allowed to range between 1 (same affinity) and
1169 10.

1170 The source code for performing the Monte Carlo simulation is available at
1171 https://github.com/shazanfar/cellAggregator, and an interactive R Shiny application
1172 available at http://shiny.maths.usyd.edu.au/cellAggregator/.

1173 **Supplemental Information**
1174
1175 **Validation of NanoString Data**
1176 *Pcdh18* data was discarded due to an error in the codeset. However, *Pcdh18* was not
1177 detected by RNA *in situ* hybridization experiments in the epithelium nor in subsequent
1178 single OSN qPCR experiments. Negative controls (e.g. water or media only) showed no
1179 signal following amplification, indicating a lack of contamination. To validate the
1180 NanoString data, we first performed a "pool-split" experiment to determine technical
1181 reproducibility. RNA from 12 single cells were pooled and then split into multiple
1182 aliquots. Each aliquot was separately amplified and processed to assess technical
1183 reproducibility. Samples showed good correlation (R^2=0.62; data not shown). Second,
1184 we asked if averaging the expression patterns from single neurons approximated the
1185 pattern seen using bulk epithelial RNA. We found strong correlation (R^2=0.65) despite
1186 the fact we only analyzed 50 cells, and bulk RNA contains neurons, glia, and other cell-
1187 types (data not shown). Finally, multiple discriminant analysis (MDA) showed that pool-
1188 split samples clustered with single cells while the water and bulk samples formed
1189 separate, discrete clusters (data not shown).
1190
1191 To address the concern that dissociation of whole epithelia would affect δ-Pcdh
1192 expression, we generated a proxy for *in vivo* expression by performing single color RNA
1193 *in situ* hybridization studies (Figure 1 - Supplement 1A-G; no signal was detected for
1194 *Pcdh11x* or *Pcdh18*). Interestingly, the pattern of expression was clearly variable among
1195 neurons, and unevenly distributed within the epithelium (Figure 1 - Supplement 1B-G).
1196 We used this RNA *in situ* data to estimate the proportion of OSNs that express each δ-

1197   Pcdh (Figure 1 - Supplement 1J; see Methods). We found that our single neuron data
1198   and these *in vivo* estimates followed similar trends (R^2=0.58), suggesting dissociation
1199   did not have an appreciable impact on our NanoString data.

1200   **Acknowledgments**

1203

1204   **Declaration of Interests**

1205   The authors declare no competing interests.

References

Chang H, Hoshina N, Zhang C, Ma Y, Cao H, Wang Y, Wu D-D, Bergen SE, Landén M, Hultman CM, Preisig M, Kutalik Z, Castelao E, Grigoroiu-Serbanescu M, Forstner AJ, Strohmaier J, Hecker J, Schulze TG, Müller-Myhsok B, Reif A, Mitchell PB, Martin NG, Schofield PR, Cichon S, Nöthen MM, Swedish Bipolar Study Group, MooDS Bipolar Consortium, Walter H, Erk S, Heinz A, Amin N, van Duijn CM, Meyer-Lindenberg A, Tost H, Xiao X, Yamamoto T, Rietschel M, Li M. 2018. The protocadherin 17 gene affects cognition, personality, amygdala structure and function, synapse development and risk of major mood disorders. *Mol Psychiatry* **23**:400–412. doi:10.1038/mp.2016.231

Chen X, Gumbiner BM. 2006. Paraxial protocadherin mediates cell sorting and tissue morphogenesis by regulating C-cadherin adhesion activity. *J Cell Biol* **174**:301–313. doi:10.1083/jcb.200602062

Chen X, Koh E, Yoder M, Gumbiner BM. 2009. A protocadherin-cadherin-FLRT3 complex controls cell adhesion and morphogenesis. *PLoS ONE* **4**:e8411. doi:10.1371/journal.pone.0008411

Chen X, Molino C, Liu L, Gumbiner BM. 2007. Structural elements necessary for oligomerization, trafficking, and cell sorting function of paraxial protocadherin. *J Biol Chem* **282**:32128–32137. doi:10.1074/jbc.M705337200

Consortium on Complex Epilepsies. 2014. Genetic determinants of common epilepsies: a meta-analysis of genome-wide association studies. *Lancet Neurol* **13**:893–903. doi:10.1016/S1474-4422(14)70171-1

Cooper SR, Emond MR, Duy PQ, Liebau BG, Wolman MA, Jontes JD. 2015. Protocadherins control the modular assembly of neuronal columns in the zebrafish optic tectum. *J Cell Biol* **211**:807–814. doi:10.1083/jcb.201507108

Cooper SR, Jontes JD, Sotomayor M. 2016. Structural determinants of adhesion by Protocadherin-19 and implications for its role in epilepsy. *Elife* **5**:335. doi:10.7554/eLife.18529

Dibbens LM, Tarpey PS, Hynes K, Bayly MA, Scheffer IE, Smith R, Bomar J, Sutton E, Vandeleur L, Shoubridge C, Edkins S, Turner SJ, Stevens C, O'Meara S, Tofts C, Barthorpe S, Buck G, Cole J, Halliday K, Jones D, Lee R, Madison M, Mironenko T, Varian J, West S, Widaa S, Wray P, Teague J, Dicks E, Butler A, Menzies A, Jenkinson A, Shepherd R, Gusella JF, Afawi Z, Mazarib A, Neufeld MY, Kivity S, Lev D, Lerman-Sagie T, Korczyn AD, Derry CP, Sutherland GR, Friend K, Shaw M, Corbett M, Kim H-G, Geschwind DH, Thomas P, Haan E, Ryan S, McKee S, Berkovic SF, Futreal PA, Stratton MR, Mulley JC, Gécz J. 2008. X-linked protocadherin 19 mutations cause female-limited epilepsy and cognitive impairment. *Nat Genet* **40**:776–781. doi:10.1038/ng.149

Emond MR, Biswas S, Blevins CJ, Jontes JD. 2011. A complex of Protocadherin-19 and N-cadherin mediates a novel mechanism of cell adhesion. *J Cell Biol* **195**:1115–1121. doi:10.1083/jcb.201108115

Emond MR, Biswas S, Jontes JD. 2009. Protocadherin-19 is essential for early steps in brain morphogenesis. *Dev Biol* **334**:72–83. doi:10.1016/j.ydbio.2009.07.008

Etzrodt J, Krishna-K K, Redies C. 2009. Expression of classic cadherins and delta-protocadherins in the developing ferret retina. *BMC Neurosci* **10**:153. doi:10.1186/1471-2202-10-153

1252 Foty RA, Steinberg MS. 2005. The differential adhesion hypothesis: a direct evaluation.
1253   *Dev Biol* **278**:255–263. doi:10.1016/j.ydbio.2004.11.012
1254 Friedlander DR, Mège RM, Cunningham BA, Edelman GM. 1989. Cell sorting-out is
1255   modulated by both the specificity and amount of different cell adhesion molecules
1256   (CAMs) expressed on cell surfaces. *Proc Natl Acad Sci USA* **86**:7043–7047.
1257 Geiss GK, Bumgarner RE, Birditt B, Dahl T, Dowidar N, Dunaway DL, Fell HP, Ferree
1258   S, George RD, Grogan T, James JJ, Maysuria M, Mitton JD, Oliveri P, Osborn JL,
1259   Peng T, Ratcliffe AL, Webster PJ, Davidson EH, Hood L, Dimitrov K. 2008. Direct
1260   multiplexed measurement of gene expression with color-coded probe pairs. *Nat*
1261   *Biotechnol* **26**:317–325. doi:10.1038/nbt1385
1262 Ghazanfar S, Bisogni AJ, Ormerod JT, Lin DM, Yang JYH. 2016. Integrated single cell
1263   data analysis reveals cell specific networks and novel coactivation markers. *BMC*
1264   *Systems Biology* **10**:127.
1265 Goodman KM, Rubinstein R, Thu CA, Mannepalli S, Bahna F, Ahlsen G, Rittenhouse C,
1266   Maniatis T, Honig B, Shapiro L. 2016. γ-Protocadherin structural diversity and
1267   functional implications. *Elife* **5**:213. doi:10.7554/eLife.20930
1268 Hanchate NK, Kondoh K, Lu Z, Kuang D, Ye X, Qiu X, Pachter L, Trapnell C, Buck LB.
1269   2015. Single-cell transcriptomics reveals receptor transformations during olfactory
1270   neurogenesis. *Science* **350**:1251–1255. doi:10.1126/science.aad2456
1271 Harrison OJ, Bahna F, Katsamba PS, Jin X, Brasch J, Vendome J, Ahlsen G, Carroll
1272   KJ, Price SR, Honig B, Shapiro L. 2010. Two-step adhesive binding by classical
1273   cadherins. *Nat Struct Mol Biol* **17**:348–357. doi:10.1038/nsmb.1784
1274 Hasegawa S, Hamada S, Kumode Y, Esumi S, Katori S, Fukuda E, Uchiyama Y,
1275   Hirabayashi T, Mombaerts P, Yagi T. 2008. The protocadherin-alpha family is
1276   involved in axonal coalescence of olfactory sensory neurons into glomeruli of the
1277   olfactory bulb in mouse. *Mol Cell Neurosci* **38**:66–79.
1278   doi:10.1016/j.mcn.2008.01.016
1279 Hayashi S, Inoue Y, Kiyonari H, Abe T, Misaki K, Moriguchi H, Tanaka Y, Takeichi M.
1280   2014. Protocadherin-17 mediates collective axon extension by recruiting actin
1281   regulator complexes to interaxonal contacts. *Dev Cell* **30**:673–687.
1282   doi:10.1016/j.devcel.2014.07.015
1283 Hirano K, Kaneko R, Izawa T, Kawaguchi M, Kitsukawa T, Yagi T. 2012. Single-neuron
1284   diversity generated by Protocadherin-β cluster in mouse central and peripheral
1285   nervous systems. *Front Mol Neurosci* **5**:90. doi:10.3389/fnmol.2012.00090
1286 Hoshina N, Tanimura A, Yamasaki M, Inoue T, Fukabori R, Kuroda T, Yokoyama K,
1287   Tezuka T, Sagara H, Hirano S, Kiyonari H, Takada M, Kobayashi K, Watanabe M,
1288   Kano M, Nakazawa T, Yamamoto T. 2013. Protocadherin 17 regulates presynaptic
1289   assembly in topographic corticobasal Ganglia circuits. *Neuron* **78**:839–854.
1290   doi:10.1016/j.neuron.2013.03.031
1291 Hulpiau P, van Roy F. 2009. Molecular evolution of the cadherin superfamily. *Int J*
1292   *Biochem Cell Biol* **41**:349–369. doi:10.1016/j.biocel.2008.09.027
1293 Ing-Esteves S, Kostadinov D, Marocha J, Sing AD, Joseph KS, Laboulaye MA, Sanes
1294   JR, Lefebvre JL. 2018. Combinatorial Effects of Alpha- and Gamma-Protocadherins
1295   on Neuronal Survival and Dendritic Self-Avoidance. *J Neurosci* **38**:2713–2729.
1296   doi:10.1523/JNEUROSCI.3035-17.2018

1297 Islam S, Kjällquist U, Moliner A, Zajac P, Fan J-B, Lönnerberg P, Linnarsson S. 2011.
1298   Characterization of the single-cell transcriptional landscape by highly multiplex RNA-
1299   seq. *Genome Res* **21**:1160–1167. doi:10.1101/gr.110882.110
1300 Katsamba P, Carroll K, Ahlsen G, Bahna F, Vendome J, Posy S, Rajebhosale M, Price
1301   S, Jessell TM, Ben-Shaul A, Shapiro L, Honig BH. 2009. Linking molecular affinity
1302   and cellular specificity in cadherin-mediated adhesion. *Proc Natl Acad Sci USA*
1303   **106**:11594–11599. doi:10.1073/pnas.0905349106
1304 Krishna-K K, Hertel N, Redies C. 2011. Cadherin expression in the somatosensory
1305   cortex: evidence for a combinatorial molecular code at the single-cell level.
1306   *Neuroscience* **175**:37–48. doi:10.1016/j.neuroscience.2010.11.056
1307 Lefebvre JL, Kostadinov D, Chen WV, Maniatis T, Sanes JR. 2012. Protocadherins
1308   mediate dendritic self-avoidance in the mammalian nervous system. *Nature*
1309   **488**:517–521. doi:10.1038/nature11305
1310 Leung LC, Urbančič V, Baudet M-L, Dwivedy A, Bayley TG, Lee AC, Harris WA, Holt
1311   CE. 2013. Coupling of NF-protocadherin signaling to axon guidance by cue-induced
1312   translation. *Nat Neurosci* **16**:166–173. doi:10.1038/nn.3290
1313 Light SEW, Jontes JD. 2017. δ-Protocadherins: Organizers of neural circuit assembly.
1314   *Semin Cell Dev Biol* **69**:83–90. doi:10.1016/j.semcdb.2017.07.037
1315 Marinov GK, Williams BA, McCue K, Schroth GP, Gertz J, Myers RM, Wold BJ. 2014.
1316   From single-cell to cell-pool transcriptomes: stochasticity in gene expression and
1317   RNA splicing. *Genome Res* **24**:496–510. doi:10.1101/gr.161034.113
1318 Molumby MJ, Keeler AB, Weiner JA. 2016. Homophilic Protocadherin Cell-Cell
1319   Interactions Promote Dendrite Complexity. *Cell Rep* **15**:1037–1050.
1320   doi:10.1016/j.celrep.2016.03.093
1321 Morrow EM, Yoo S-Y, Flavell SW, Kim T-K, Lin Y, Hill RS, Mukaddes NM, Balkhy S,
1322   Gascon G, Hashmi A, Al-Saad S, Ware J, Joseph RM, Greenblatt R, Gleason D,
1323   Ertelt JA, Apse KA, Bodell A, Partlow JN, Barry B, Yao H, Markianos K, Ferland RJ,
1324   Greenberg ME, Walsh CA. 2008. Identifying autism loci and genes by tracing recent
1325   shared ancestry. *Science* **321**:218–223. doi:10.1126/science.1157657
1326 Mountoufaris G, Chen WV, Hirabayashi Y, O'Keeffe S, Chevee M, Nwakeze CL, Polleux
1327   F, Maniatis T. 2017. Multicluster Pcdh diversity is required for mouse olfactory
1328   neural circuit assembly. *Science* **356**:411–414. doi:10.1126/science.aai8801
1329 Nollet F, Kools P, van Roy F. 2000. Phylogenetic analysis of the cadherin superfamily
1330   allows identification of six major subfamilies besides several solitary members. *J*
1331   *Mol Biol* **299**:551–572. doi:10.1006/jmbi.2000.3777
1332 Ozawa M, Kemler R. 1998. Altered cell adhesion activity by pervanadate due to the
1333   dissociation of alpha-catenin from the E-cadherin.catenin complex. *J Biol Chem*
1334   **273**:6166–6170.
1335 Pederick DT, Richards KL, Piltz SG, Kumar R, Mincheva-Tasheva S, Mandelstam SA,
1336   Dale RC, Scheffer IE, Gécz J, Petrou S, Hughes JN, Thomas PQ. 2018. Abnormal
1337   Cell Sorting Underlies the Unique X-Linked Inheritance of PCDH19 Epilepsy.
1338   *Neuron* **97**:59–66.e5. doi:10.1016/j.neuron.2017.12.005
1339 Redies C, Vanhalst K, Roy FV. 2005. delta-Protocadherins: unique structures and
1340   functions. *Cell Mol Life Sci* **62**:2840–2852. doi:10.1007/s00018-005-5320-z

1341   Ressler KJ, Sullivan SL, Buck LB. 1994. Information coding in the olfactory system:
1342   evidence for a stereotyped and highly organized epitope map in the olfactory bulb.
1343   *Cell* **79**:1245–1255.
1344   Rubinstein R, Goodman KM, Maniatis T, Shapiro L, Honig B. 2017. Structural origins of
1345   clustered protocadherin-mediated neuronal barcoding. *Semin Cell Dev Biol* **69**:140–
1346   150. doi:10.1016/j.semcdb.2017.07.023
1347   Rubinstein R, Thu CA, Goodman KM, Wolcott HN, Bahna F, Mannepalli S, Ahlsen G,
1348   Chevee M, Halim A, Clausen H, Maniatis T, Shapiro L, Honig B. 2015. Molecular
1349   Logic of Neuronal Self-Recognition through Protocadherin Domain Interactions. *Cell*
1350   **163**:629–642. doi:10.1016/j.cell.2015.09.026
1351   Saraiva LR, Ibarra-Soria X, Khan M, Omura M, Scialdone A, Mombaerts P, Marioni JC,
1352   Logan DW. 2015. Hierarchical deconstruction of mouse olfactory sensory neurons:
1353   from whole mucosa to single-cell RNA-seq. *Sci Rep* **5**:18178.
1354   doi:10.1038/srep18178
1355   Schreiner D, Weiner JA. 2010. Combinatorial homophilic interaction between gamma-
1356   protocadherin multimers greatly expands the molecular diversity of cell adhesion.
1357   *Proc Natl Acad Sci USA* **107**:14893–14898. doi:10.1073/pnas.1004526107
1358   Steinberg MS, Takeichi M. 1994. Experimental specification of cell sorting, tissue
1359   spreading, and specific spatial patterning by quantitative differences in cadherin
1360   expression. *Proc Natl Acad Sci USA* **91**:206–209.
1361   Tan L, Li Q, Xie XS. 2015. Olfactory sensory neurons transiently express multiple
1362   olfactory receptors during development. *Mol Syst Biol* **11**:844–844.
1363   doi:10.15252/msb.20156639
1364   Thu CA, Chen WV, Rubinstein R, Chevee M, Wolcott HN, Felsovalyi KO, Tapia JC,
1365   Shapiro L, Honig B, Maniatis T. 2014. Single-cell identity generated by combinatorial
1366   homophilic interactions between α, β, and γ protocadherins. *Cell* **158**:1045–1059.
1367   doi:10.1016/j.cell.2014.07.012
1368   Uemura M, Nakao S, Suzuki ST, Takeichi M, Hirano S. 2007. OL-Protocadherin is
1369   essential for growth of striatal axons and thalamocortical projections. *Nat Neurosci*
1370   **10**:1151–1159. doi:10.1038/nn1960
1371   Vanhalst K, Kools P, Staes K, van Roy F, Redies C. 2005. delta-Protocadherins: a gene
1372   family expressed differentially in the mouse brain. *Cell Mol Life Sci* **62**:1247–1259.
1373   doi:10.1007/s00018-005-5021-7
1374   Vassar R, Chao SK, Sitcheran R, Nuñez JM, Vosshall LB, Axel R. 1994. Topographic
1375   organization of sensory projections to the olfactory bulb. *Cell* **79**:981–991.
1376   Wang X, Weiner JA, Levi S, Craig AM, Bradley A, Sanes JR. 2002. Gamma
1377   protocadherins are required for survival of spinal interneurons. *Neuron* **36**:843–854.
1378   Weiner JA, Wang X, Tapia JC, Sanes JR. 2005. Gamma protocadherins are required
1379   for synaptic development in the spinal cord. *Proc Natl Acad Sci USA* **102**:8–14.
1380   doi:10.1073/pnas.0407931101
1381   Williams EO, Sickles HM, Dooley AL, Palumbos S, Bisogni AJ, Lin DM. 2011. Delta
1382   Protocadherin 10 is Regulated by Activity in the Mouse Main Olfactory System.
1383   *Front Neural Circuits* **5**:9. doi:10.3389/fncir.2011.00009
1384